Gasdermin-D-dependent IL-1α release from microglia promotes protective immunity during chronic *Toxoplasma gondii* infection

Samantha J. Batista[1], Katherine M. Still[1], David Johanson[1], Jeremy A. Thompson[1], Carleigh A. O'Brien[1], John R. Lukens[1], and Tajie H. Harris[1*]

Affiliations: [1]Center for Brain Immunology and Glia, Department of Neuroscience, University of Virginia, Charlottesville, VA 22908.

Corresponding Author and Lead Contact:

Tajie H. Harris

MR-4 Room 6148

409 Lane Road

Charlottesville, VA 22903

Phone: 434-982-6916

Fax: 434-982-4380

Email: tajieharris@virginia.edu

This work was funded by National Institutes of Health grants R01NS091067 and R56NS106028 to T.H.H., R01NS106383 to J.R.L., T32AI007046 to S.J.B., T32GM008328 to K.M.S., and T32AI007496 to C.A.O., as well as the Carter Immunology Center Collaborative Research Grant to T.H.H., The Alzheimer's Association grant AARG-18-566113 to J.R.L., The Owens Family Foundation to J.R.L., and The University of Virginia R&D Award to J.R.L..

Abstract

Microglia, the resident immune cells of the brain parenchyma, are thought to be first-line defenders against CNS infections. We sought to identify specific roles of microglia in the control of the eukaryotic parasite *Toxoplasma gondii*, an opportunistic infection that can cause severe neurological disease. In order to identify the specific function of microglia in the brain during infection, we sorted microglia and infiltrating myeloid cells from infected microglia reporter mice. Using RNA-sequencing, we find strong NF-κB and inflammatory cytokine signatures overrepresented in blood-derived macrophages versus microglia. Interestingly, we also find that IL-1α is enriched in microglia and IL-1β in macrophages, which was also evident at the protein level. We find that mice lacking IL-1R1 or IL-1α, but not IL-1β, have impaired parasite control and immune cell infiltration specifically within the brain. Further, by sorting purified populations from infected brains, we show that microglia, not peripheral myeloid cells, release IL-1α *ex vivo*. Finally, using knockout mice as well as chemical inhibition, we show that *ex vivo* IL-1α release is gasdermin-D dependent, and that gasdermin-D and caspase-1/11 deficient mice show deficits in immune infiltration into the brain and parasite control. These results demonstrate that microglia and macrophages are differently equipped to propagate inflammation, and that in chronic *T. gondii* infection, microglia specifically can release the alarmin IL-1α, a cytokine that promotes neuroinflammation and parasite control.

INTRODUCTION

Numerous brain infections cause significant morbidity and mortality worldwide. Many of these pathogens persist in a chronic latent form in the brain and require constant immune pressure to prevent symptomatic disease. As the only resident immune cell, microglia are widely assumed to play an integral role in controlling CNS infections, but in many contexts their specific role remains poorly understood. One CNS-tropic pathogen is *Toxoplasma gondii*, a eukaryotic parasite with a broad host range that infects a large portion of the human population.[1-6] *T. gondii* establishes chronic infections by encysting in immune privileged organs, including the brain.[7,8] Without sufficient immune pressure, an often fatal neurological manifestation of this disease toxoplasmic encephalitis can occur.[2,5,6]

Studies done in mice, a natural host of this parasite, have elucidated many aspects of the immune response that are essential for maintaining control of the parasite during chronic stages of infection. T cell-derived IFN-γ is one essential element.[9-11] IFN-γ acts on target cells to induce an anti-parasitic state, allowing for the destruction of the parasite through a number of mechanisms including the recruitment of immunity-related GTPases (IRGs) and guanylate binding proteins (GBPs) to the parasitophorous vacuole, as well as the production of nitric oxide (NO).[12-17] Large numbers of monocytes and monocyte-derived macrophages, a target population for IFN-γ signaling,[13] are recruited into the brain parenchyma during chronic *T. gondii* infection in mice, and these cells are also necessary for maintaining control of the parasite and host survival.[18] Though microglia occupy the same environment as these cells in the infected brain, have an activated morphology, their role in chronic *T. gondii* infection has not been fully elucidated. Indeed, whether microglia and recruited macrophages respond in similar ways to brain infection is an open question.

In this work, we have focused on IL-1, its expression by microglia and macrophages, as well as its role in the brain during chronic *T. gondii* infection. IL-1 molecules include two main cytokines: IL-1α and IL-1β. IL-1α can function as a canonical alarmin, which is a pre-stored molecule that does not require processing and can be released upon cell death or damage, making it an ideal candidate for an early initiator of inflammation.[19,20] In contrast, IL-1β is produced first as a pro-form that requires cleavage by caspase-1 in order for it to be biologically active, rendering IL-1β dependent on the inflammasome as a platform for caspase-1 activation.[21-23] Both of these cytokines signal through the same receptor (IL-1R), a heterodimer of IL-1R1 and IL-1RAcP, with similar affinity.[24] They also lack signal sequences and thus require a loss of membrane integrity to be released. Caspase-mediate cleavage of gasdermin molecules has been identified as a major pathway leading to pore formation and IL-1 release.

The role of IL-1β and inflammasome pathways in *T. gondii* infection has been studied *in vitro* as well as in rodent models of acute infection. In sum, these studies suggest roles for IL-1β, IL18, IL-1R, NLRP1 and/or NLPR3 inflammasome sensors, the inflammasome adaptor protein ASC, and inflammatory caspases-1 and -11.[25-28] However, the role of IL-1 signaling in the brain during chronic infection has not been addressed.

Here, we show that though they are present in the same tissue microenvironment in the brain during *T. gondii* infection, monocyte-derived macrophages in the brain have a stronger NF-κB signature than brain-resident microglia. Interestingly, we also find that while IL-1α is enriched in microglia, IL-1β is overrepresented in macrophages, suggesting that these two cell types are able to contribute to IL-1-driven inflammation in different ways. We go on to show that IL-1 signaling is, indeed, important in this model as *Il1r1*$^{-/-}$ mice chronically infected with *T. gondii* are less able to control parasite in the brain, and additionally, these mice have deficits in the

recruitment of inflammatory monocytes and macrophages into the brain in comparison to wild-type mice. We find IL-1R1 expression predominantly on blood vasculature in the brain, and observe IL-1-dependent activation of the vasculature during infection. Further, IL-1-dependent control of *T. gondii* is mediated though IL-1R1 expression on a radio-resistant cell population. Interestingly, the pro-inflammatory effect of IL-1 signaling is mediated via the alarmin IL-1α, not IL-1β. We show that microglia, but not infiltrating macrophages, release IL-1α *ex vivo* in an infection- and gasdermin-D-dependent manner. We propose that one specific function of microglia during *T. gondii* infection is to release the alarmin IL-1α to promote protective neuroinflammation and parasite control.

RESULTS

Microglia lack a broad inflammatory signature compared to macrophages in the infected brain

As the resident macrophages in the brain microglia are assumed to play a significant role in infections and insults to the brain. *T. gondii* infection results in robust, sustained brain inflammation that is necessary for parasite control. This inflammation in marked by the infiltration of blood-derived T cells and monocytes into the brain as well as morphological activation of microglia. Blood-derived monocytes have been demonstrated to be important for host survival during infection[18], but whether microglia perform similar functions is still unknown. Previous work from our lab has observed that while blood-derived monocytes and macrophages express high levels of the nitric oxide-generating enzyme iNOS in the brain during *T. gondii* infection, microglia markedly lack this anti-parasitic molecule.[29] This observation led to the hypothesis that even though they are in the same tissue microenvironment, microglia are unable to respond to the

116 infection in the same way as infiltrating macrophages. Thus, we used a CX3CR1$^{Cre-ERT2}$ x
117 ZsGreen$^{fl/stop/fl}$ mouse line that has been previously described as a microglia reporter line.[30]
118 Reporter mice were treated with tamoxifen to induce ZsGreen expression and rested for 4 weeks
119 after tamoxifen injection to ensure turnover of peripheral CX3CR1-expressing cells. We have
120 consistently used this mouse line in our lab to label over 98% of microglia in the brain. Perivascular
121 macrophages will also be labeled by this method, but are not purified by our isolation protocol as
122 evidenced by a lack of CD206^{+} cells. Following infection, FACS was used to sort out
123 CD45^{+}CD11b^{+} ZsGreen^{+} microglia and ZsGreen^{-} blood-derived myeloid cells from brains of
124 infected mice for RNA sequencing analysis (Fig. 1a).

125 Analysis of differentially expressed genes shows that these two cell populations segregate
126 clearly from each other, confirming that they are fundamentally different cell types (Fig. 1b).
127 Analysis of pathway enrichment displayed a striking lack of an inflammatory signature in
128 microglia compared to macrophages (Fig. 1c), and we further show a selection of genes that were
129 differentially expressed, showing a clear enrichment for inflammation associated genes in the
130 macrophage population (Fig. 1d). Interestingly, an NF-κB signature seemed to be one factor
131 differentiating the macrophages from the microglia (Fig. 1c-d). A difference in expression of NF-
132 κB genes could provide the basis for functional differences between microglia and macrophages
133 and their ability to respond to the infection. Thus, we aimed to validate this at the protein level in
134 infected mice. Indeed, in brain sections from infected microglia reporter mice, both RelA and Rel
135 were distinctly absent from ZsGreen^{+} microglia (Fig. 1e-f) but these molecules were present in
136 ZsGreen^{-}Iba1^{+} macrophages (Fig. 1g-h). This suggests that some aspects of microglia identity may
137 inhibit upregulation of a certain inflammatory signature during infection, including a strong NF-
138 κB response.
139

IL-1 genes are differentially expressed by microglia and macrophages

The sequencing data showed that many inflammatory cytokine and chemokine signatures were also enriched in the macrophages compared to the microglia. Of note, it was observed that the IL-1 cytokines segregated differently between these populations. IL-1α was enriched in the microglia population, while IL-1β was enriched in the macrophage population (Fig. 1d). This suggests that these two cell types may be differently equipped to propagate innate inflammatory signals. The lack of microglia expression of pro-IL-1β was validated at the protein level in sections from infected microglia reporter mice, which also showed its expression by ZsGreen^{-}Iba1^{+} cells (Fig. 1i-j). On the other hand, staining of tissue sections from chronically infected microglia reporter mice show IL-1α expression generally in Iba1^{+} cells (Fig. 1k), and further confirm microglial expression of IL-1α (Fig. 1l). These results were further confirmed using flow cytometry analysis on the brains of both WT and microglia reporter mice. IL-1α protein is present in the brain prior to infection where it is found in ZsGreen^{+} microglia and microglia defined by CD11b^{+}CD45^{int} (Fig. S1a-b,d). During chronic infection, it is expressed by both ZsGreen^{+} microglia and ZsGreen^{-} myeloid cells (Fig. S1b) also defined by CD11b^{+}CD45^{int} and CD45^{hi} (Fig. S1f). IL-1β was not detected in uninfected brains, but was detected in the brain during chronic *T. gondii* infection (Fig. S1b,f). During chronic infection, pro-IL-1β and was not significantly expressed by ZsGreen^{+} cells, but was rather seen in ZsGreen^{-} myeloid cells (Fig. S1c) also defined as CD11b^{+}CD45^{hi} cells (Fig. S1g). It was also apparent that while ZsGreen^{-} blood-derived myeloid cells can express both IL-1α and pro-IL-1β, very few ZsGreen^{+} microglia were double positive (Fig. S1d). These data suggested that microglia and macrophages may play different roles in an IL-1 response. Thus, we aimed to investigate the potential importance of an IL-1 response in *T. gondii* infection.

Il1r1$^{-/-}$ mice have an impaired immune response to *T. gondii* infection

To determine if IL-1 signaling plays a role in chronic *T. gondii* infection, we infected mice lacking the IL-1 receptor (IL-1R1), which is bound by both IL-1α and IL-1β. Six weeks post-infection (p.i.) *Il1r1*$^{-/-}$ mice displayed an increase in parasite cyst burden in the brain (Fig. 2a). An increase in parasite burden is often due to impaired immune responses. Indeed, *Il1r1*$^{-/-}$ mice also have a decrease in the number of CD11b^{+}CD45^{hi} cells of the monocyte/macrophage lineage in the brain during chronic infection (Fig. 2b, f-g). Microglia typically express intermediate levels of CD45 compared to the high levels expressed by blood-derived myeloid cells, thus we use this marker as a proxy to define these populations by flow cytometry.[31] The cells we defined as infiltrating monocyte/macrophages are also Ly6G^{-}, CD11c^{-}, and Ly6C^{+}. Infiltrating myeloid cells are important producers of nitric oxide, a key anti-parasitic molecule, and thus we assessed their expression of inducible nitric oxide synthase (iNOS). *Il1r1*$^{-/-}$ mice had significantly decreased expression of iNOS in the brain compared to WT mice (Fig. 2c, h-i), which was observed specifically in focal areas of inflammation (Fig. 2j-k). Of note, though there were decreases in CD4^{+} and CD8^{+} T cells (Fig. 2d-e), the reduced iNOS expression did not appear to be due to reductions in IFN-γ production from the T cell compartment within the brain, which was unchanged between groups (Fig. S2a-b). Together, these data suggest that the CNS immune response is affected in *Il1r1*$^{-/-}$ mice, with striking deficits particularly in the myeloid response.

Importantly, these differences were restricted to the site of infection, as there were no deficits in any immune cell compartments in the spleens of *Il1r1*$^{-/-}$ mice (Fig. S2c-h). In fact, T cell and macrophage responses were slightly elevated in the spleen. The immune deficits in *Il1r1*$^{-/-}$ mice are also specific to chronic infection as *Il1r1*$^{-/-}$ mice analyzed earlier during infection (12 dpi) displayed no deficit in their monocyte/macrophage or T cell populations compared to WT in the peritoneal cavity or the spleen (Fig. S3a-b). IFN-γ levels in the serum were,

if anything, increased in *Il1r1*$^{-/-}$ mice at this time point, indicating that this response is not impaired (Fig. S3c). The only immune defect detected during this early phase of infection in *Il1r1*$^{-/-}$ mice was a decrease in neutrophils recruited to the peritoneal cavity (Fig. S3a). In sum, these results show that mice lacking IL-1R1 have an impaired response of blood-derived immune cells in the brain, leading to increased parasite burden. This suggests that IL-1 signaling promotes immune responses in the brain during chronic *T. gondii* infection.

IL-1R1 is expressed by brain vasculature during chronic *T. gondii* infection

Having established a role for IL-1 signaling in promoting the immune response to chronic *T. gondii* infection in the brain, we next wanted to determine which cells in the brain could respond to IL-1 in the brain environment. We performed immunohistochemical staining for IL-1R1 on brain sections from chronically infected mice. We found that IL-1R1 was expressed principally on blood vessels in the brain, as marked by laminin staining which highlights basement membranes of blood vessels (Fig. 3a-b). Interestingly, expression is not seen continuously along vessels (Fig. 3a-b), nor on all vessels (Fig. 3b). This suggests a degree of heterogeneity among endothelial cells and perhaps in their ability to respond to IL-1. We detected IL-1R1 expression specifically on CD31^{+} cells by IHC (Fig. S4a) and by flow cytometry (Fig. S4b-c). To test whether endothelial expression of IL-1R1 is required in this infection, we first assessed potential contributions from radiosensitive (hematopoietic) and radio-resistant (non-hematopoietic) cells. To do this, we created bone marrow chimeras with *Il1r1*$^{-/-}$ mice. We lethally irradiated both WT and *Il1r1*$^{-/-}$ mice, and then i.v. transferred bone marrow cells from either WT or *Il1r1*$^{-/-}$ mice. We allowed 6 weeks for reconstitution before infecting the mice with *T. gondii*, and we performed our analyses at 4 weeks post infection (Fig. 3c). We found that *Il1r1*$^{-/-}$ recipients that had received WT

bone marrow, had a higher cyst burden in their brain than WT recipients that had received either WT or *Il1r1*$^{-/-}$ bone marrow (Fig. 3d). Consistent with this, *Il1r1*$^{-/-}$ recipient mice, regardless of their source of bone marrow displayed a decrease in total leukocyte numbers in the brain compared to WT recipients (Fig. 3e). Taken together, these data suggest that IL-1R1 expression on a radio-resistant cell population is required for host control of the parasite, which is consistent with our hypothesis that the relevant expression is on brain endothelial cells.

Vascular adhesion molecule expression in the brain is partially dependent on IL-1R1 signaling and is necessary for monocyte infiltration

During chronic *T. gondii* infection continual infiltration of immune cells into the brain is necessary for maintaining control of the parasite. One step in getting cells to successfully infiltrate the brain, as in other tissues, is the interaction with activated endothelium expressing vascular adhesion molecules as well as chemokines. Indeed, the brain endothelium is activated during chronic *T. gondii* infection compared to the naïve state, as seen by increased expression of ICAM-1 and VCAM-1 molecules on brain endothelial cells (Fig. S5a-d). Our data show that ICAM-1 is expressed to a higher extent by endothelial cells that express IL-1R1 compared to cells that do not in the naïve state (Fig. S5e), and that IL-1R1^{+} endothelial cells also express VCAM-1 in infected tissues (Fig. S5f).

We investigated the dependence of these molecules on IL-1 signaling in our model, and found that their expression is dependent in part on IL-1 signaling. *Il1r1*$^{-/-}$ mice displayed decreased mRNA expression of *Icam1*, *Vcam1*, and *Ccl2* in the brain (Fig. 3f) as assessed using whole brain homogenate from chronically infected mice. To more specifically address effects on the CNS vasculature, we examined expression of ICAM-1 and VCAM-1 protein in brain sections of WT

and *Il1r1*$^{-/-}$ mice during chronic infection using IHC (Fig. 3g-j). Representative images show a marked decrease in ICAM-1 and VCAM-1 reactivity on blood vessels in the brains of *Il1r1*$^{-/-}$ mice compared to WT (Fig. 3g-j). Together, these data show that the increased expression of vascular adhesion molecules, and potentially chemokine, in the brain that is characteristic of chronic *T. gondii* infection is partially dependent on IL-1 signaling. The modulation of adhesion molecule expression may be one mechanism by which IL-1 promotes the infiltration of immune into the brain during chronic *T. gondii* infection.

To determine the importance of ICAM-1 and VCAM-1 in the recruitment of infiltrating monocytes during chronic *T. gondii* infection, we used antibody treatments to block their ligands (LFA-1 and VLA-4 respectively) *in vivo*. We treated chronically infected WT mice with a combination of α-LFA-1 and α-VLA-4 blocking antibodies, giving a total of two treatments. After 5 days of treatment, mice receiving blocking antibody displayed decreases in the number of infiltrating myeloid cells isolated from the brain compared to control treated mice (Fig. S5g). Specifically, we observed deficits in the Ly6C^{hi} population (Fig. S5h), indicating a lack of blood-derived monocytes. The decrease in monocyte entry translated into fewer iNOS^{+} cells in the brain as well (Fig. S5i). These data show that interactions with ICAM-1 and VCAM-1 are necessary for monocyte infiltration into the brain during chronic infection, and that IL-1 signaling promotes the expression of these adhesion molecules.

IL-1α$^{-/-}$ but not IL-1β$^{-/-}$ mice have an impaired immune response to *T. gondii* infection

IL-1α and IL-1β both bind to and signal through IL-1R1. Having established a role for IL-1 signaling in promoting the myeloid response in the brain during chronic *T. gondii* infection, we next sought to determine whether this effect was mediated by one or both of these cytokines, given

255 that IL-1α and IL-1β are expressed by different populations of myeloid cells in the infected brain.
256 To address this, we infected mice lacking either IL-1α or IL-1β and analyzed the cellular immune
257 response and parasite burden during chronic phase of infection. At six weeks post-infection, IL-
258 $1\alpha^{-/-}$ mice displayed an increase in parasite burden compared to WT as measured by qPCR analysis
259 of parasite DNA from brain homogenate (Fig. 4a). IL-$1\beta^{-/-}$ mice, however, showed no change in
260 parasite burden compared to WT (Fig. 4a). This suggests that, rather unexpectedly, IL-1α is
261 involved in maintaining control of the parasite during chronic infection, while IL-1β is not.
262 IL-$1\alpha^{-/-}$ mice displayed fewer focal areas of inflammation compared to WT (Fig. 4b-c), as
263 seen by clusters of immune cells in H&E stained brain sections. We further found that IL-$1\alpha^{-/-}$
264 mice, like *Il1r1*$^{-/-}$ mice, have decreases in peripheral monocyte/macrophage populations infiltrating
265 the brain as well as a decrease in the number of iNOS-expressing cells compared to WT (Fig. 4d-
266 e). They also had a decrease in $CD8^+$ T cells in the brain (Fig. 4f-g). On the other hand, IL-$1\beta^{-/-}$
267 mice displayed no difference from WT in the number of peripheral myeloid cells infiltrating the
268 brain during chronic infection, or in the number of these cells that are expressing iNOS across
269 multiple experiments (Fig. 4h-i), which is consistent with no change in parasite burden in these
270 mice. IL-$1\beta^{-/-}$ mice also showed no defect in T cell infiltration (Fig. 4j-k). Together, these results
271 suggest that the role of IL-1 signaling in promoting immune responses in the brain during chronic
272 *T. gondii* infection is mediated by IL-1α, rather than by IL-1β.
273
274 **IL-1α is released *ex vivo* from microglia isolated from *T. gondii* infected brains**
275 Our results demonstrate a role for IL-1α in chronic *T. gondii* infection. We have also shown that
276 microglia in the infected brain are enriched in IL-1α compared to macrophages, though it is
277 expressed by both populations. Thus, we aimed to determine which cell type releases IL-1α in this

model. Uninfected mice treated with PLX5622 for 12 days to deplete microglia lost almost all IL-1α mRNA expression in the brain (Fig. 5a), consistent with flow cytometry and immunohistochemistry data detecting IL-1α in microglia in naïve mice (Fig. S1a-b,d). To further examine IL-1α release during infection, we first established an assay to measure IL-1α release from isolated brain cells *ex vivo*. A single cell suspension was generated from brain homogenate, brain mononuclear cells were washed and plated in complete media for 18 hours, and supernatant was collected for analysis by ELISA. Using this method, we found that cells isolated from mouse brain can indeed release IL-1α in an infection-dependent manner (Fig. 5b). It should be noted that isolated spleen cells from infected animals did not release detectable IL-1α. We then used our microglia reporter model to FACS sort ZsGreen^{+} microglia and ZsGreen^{-} myeloid cells from infected mice. Equal numbers of microglia and peripheral myeloid cells were plated and supernatant was collected to measure IL-1α release. We observed a very clear difference in these populations; purified microglia released IL-1α *ex vivo*, while purified monocytes/macrophages released negligible amounts of this cytokine (Fig. 5c). We show that this difference in IL-1α release does not appear to do due to overall increased death in microglia *ex vivo* as blood-derived cells actually released more LDH (Fig. 5d). We also show that IL-1α release is inhibited when membrane integrity is preserved with glycine treatment (Fig. 5e) as well the total possible IL-1α release from isolated brain mononuclear cells *ex vivo* (Fig. 5f). Taken together, these findings show that microglia from infected mice have the capability to release IL-1α, which could suggest that microglia and macrophages may undergo different types cell death.

Caspase-1/11$^{-/-}$ mice have an impaired response to *T. gondii* infection

To begin to address whether inflammatory cell death could release IL-1α in the brain during chronic *T. gondii* infection, we first took a broad look at cell death in the brain. 4 weeks p.i., mice were injected intraperitoneally (i.p.) with propidium iodide (PI). 24 hours after PI injection, mice were sacrificed for analysis. PI uptake in cells, which is indicative of cell death or severe membrane damage, was observed in the brains of *T. gondii* infected mice, and appeared in focal areas (Fig. 6a-b), suggesting that there is cell death occurring in the brain during chronic infection.

Inflammasome activation has been implicated *in vitro* and during acute *T. gondii* infection, and could potentially be involved in IL-1α release. IL-1α, like IL-1β, is not canonically secreted and requires cell death or significant membrane perturbation to be released extracellularly.[20,32-34] Unlike IL-1β, IL-1α does not need to be processed by the inflammasome platform for its activity, however, because permeabilization of the plasma membrane is required for IL-1α to be released, inflammasome-mediated cell death may still contribute to its release. To look for evidence of inflammasome activation the brains of mice chronically infected with *T. gondii*, we infected ASC-citrine reporter mice, in which the inflammasome adaptor protein apoptosis-associated speck-like protein containing CARD (ASC) is fused with the fluorescent protein citrine. Upon inflammasome activation, the reporter shows speck-like aggregates of tagged ASC. In the brain during chronic *T. gondii* infection, ASC specks were observed around areas of inflammation in Iba1^{+} microglia or macrophages (Fig. 6c). We further crossed the ASC-citrine mouse line to the microglia reporter mouse line. Following infection, ASC specks were observed contained within microglia in the infected brain (Fig. 6d).

To further investigate a role for inflammasome-dependent processes in chronic *T. gondii* infection, we infected caspase-1/11$^{-/-}$ mice. Six weeks p.i., mice lacking these inflammatory caspases had an increased number of parasite cysts in their brains (Fig. 6e), indicating impaired

parasite control. Caspase-1/11$^{-/-}$ mice also have a decrease in the number of cells of the monocyte/macrophage lineage in the brain during chronic infection (Fig. 6f), as well as significantly fewer infiltrating myeloid cells expressing iNOS in the brain compared to WT mice (Fig. 6g). These mice also displayed decreases in CD4^{+} T cells (Fig. 6h-i). In addition to an increased overall cyst burden, caspase-1/11$^{-/-}$mice had more instances of clusters of parasite cysts compared to WT (Fig. 6j-k), likely indicating a lack of parasite control in areas of parasite reactivation. Together, these results are similar to those observed in infected *Il1r1*$^{-/-}$ mice and show that caspase-1/11 activity is important for host control of *T. gondii* infection.

Gasdermin-D$^{-/-}$ mice have an impaired response to *T. gondii* infection and impaired IL-1α release

Our data implicate an inflammasome-dependent processes in the control of *T. gondii* in the brain, thus we investigated the importance of gasdermin-D, the pore-forming executor of pyroptosis.[23,35-37] We utilized gasdermin-D (gsdmd)$^{-/-}$ mice to specifically assess the importance of pyroptosis. Six weeks p.i., gsdmd$^{-/-}$ mice displayed a significant increase in parasite cyst burden compared to WT (Fig. 7a). Like *Il1r1*$^{-/-}$, IL-1α$^{-/-}$, and caspase-1/11$^{-/-}$ mice, gsdmd$^{-/-}$ mice also displayed a decrease in the number of immune cells infiltrating the brain (Fig. 7b).

To directly assess the contribution of pyroptosis to IL-1α release, brain mononuclear cells were isolated from gsdmd$^{-/-}$ mice and *ex vivo* IL-1α release was determined by ELISA. Cells isolated from the brains of gsdmd$^{-/-}$ mice released significantly less IL-1α into the supernatant than cells from WT mice, about a 70 percent reduction in IL-1α release (Fig. 7c). We also utilized necrosulfonamide (NSA), which has been shown to be a specific inhibitor of gsdmd in mice.[38] Brain cells isolated from WT mice were analyzed for *ex vivo* IL-1α release under control

conditions, or incubated with 20μM NSA (Fig. 7d). Strikingly, NSA inhibited *ex vivo* IL-1α release, indicating that release is dependent on gsdmd. Taken together, these results suggest that IL-1α is released from cells from infected brains in a gsdmd$^{-/-}$-dependent manner, and promotes the infiltration of anti-parasitic immune cells into the *T. gondii* infected brain.

DISCUSSION

Toxoplasma gondii establishes a chronic brain infection in its host, necessitating long-term neuroinflammation.[5,6,39] Much is known about the immune response to this parasite, but the role of the brain-resident microglia is still largely unknown. Early studies using culture systems of murine and human microglia showed that IFN-γ and LPS treatment prior to infection inhibited parasite replication.[40-42] However, understanding of microglia-specific functions in brain infections has been hindered by the fact that microglia rapidly lose their identity in culture.[43] Moreover, culture techniques do not recapitulate the complex interactions microglia have during infection with other cells or the tissue architecture of the brain. Thus, we aimed to examine microglia and macrophages within the brain to begin to uncover their function.

Through RNA-seq analysis as well as staining of infected brain tissue, we find that there is an NF-κB signature present in brain-infiltrating monocytes/macrophages, that is largely absent in microglia in the same environment. These two cell types are likely exposed to the same signals within the brain, which suggests that the ontogeny of these cells has long lasting implications for their functional capacity. Transcription factors, including *Sall1*, that have been accepted as defining microglia identity may be shaping the transcriptional landscape, repressing certain loci that could potentially lead to damaging inflammation in the brain.[44] We suggest that these differences are evidence of a division of labor, with microglia and blood-derived macrophages

contributing in different ways to inflammation in the brain during infection with *T. gondii*. While blood-derived cells display a classic inflammation associated NF-κB response, microglia may be better suited to contributing to inflammation through the release of alarmins, rather than through upregulation of a broader NF-κB-dependent program that may be injurious to the local tissue.

We find the alarmin IL-1α expressed in microglia, though they notably lack expression of IL-1β which is found in infiltrating myeloid cells. This suggests that both of these cell types may be able to participate in an IL-1 response, but in fundamentally different ways. Importantly, we show that host immunity is dependent on the activity of IL-1α rather than IL-1β, and that IL-1α is released *ex vivo* from microglia but not from infiltrating macrophages. In general, IL-1β has been the subject of more study than IL-1α, and has a history of being implicated when IL-1 signaling is discussed. More recently, IL-1α has been shown to contribute to certain inflammatory environments. IL-1α release from lymph node macrophages in an inflammasome-independent death event has been shown to enhance antigen presentation and humoral responses to influenza vaccination.[45] IL-1α has been shown to initiate lung inflammation in a model of sterile inflammation using silica.[46] Recently, some reports have suggested IL-1α rather than IL-1β drives sepsis pathology.[47] IL-1α activity in the CNS has begun to be studied, with a deleterious role for the cytokine shown in spinal cord injury.[48] IL-1β has been implicated in some infection models, but IL-1α activity in brain infection has not previously been reported. As an alarmin expressed in the brain at baseline, IL-1α is ideally placed to initiate inflammation in response to early damage caused by the parasite before there is robust immune infiltration.

In this work, we also show that IL-1α likely signals on brain vasculature, promoting the infiltration of immune cells. We found that IL-1R1 expression on brain vasculature displays a

mosaic pattern. This could suggest that there are functionally distinct sub-populations of endothelial cells capable of becoming activated in response to different signals.[49] There is ample evidence in the literature to support IL-1R1 expression on endothelial cells as well as the responsiveness of CNS vasculature to IL-1.[50-55] However, IL-1 has also been shown to signal on immune cells.[56-59] We found that IL-1R1 expression on radio-resistant cells is what is important in our model, which is supportive of endothelial cells being the relevant responders, but there has also been evidence put forth that other brain resident cells can respond to IL-1. It has been suggested that microglial IL-1R1 expression plays a role in self-renewal after ablation.[60] Microglia are partially radio-resistant and do experience some turnover after irradiation and repopulation. It has also been suggested that IL-1 can act on neurons, though it should be noted that it has also been reported that neurons express a unique form of IL-1RAcP which affects downstream signaling.[61] It is unclear whether astrocytes express IL-1R1, but astrocytes represent another radio-resistant cell population in the brain that has the ability to affect immune cell infiltration through chemokine production.[29,62]

Infiltrating immune cells express pro-IL-1β but we have not detected a role for IL-1β in promoting inflammation in this model. We have also shown that they do not release IL-1α *ex vivo* even though they express it, suggesting that they may die in an immunologically quiet way such as apoptosis, while microglia may undergo a more inflammatory form of cell death, including pyroptosis. If these two cell types do in fact undergo different forms of cell death, it is of great interest how microglia activate gasdermin-D to release inflammatory factors. It is possible that microglia in an area of parasite reactivation in the brain become infected, sense parasite products in the cytoplasm, and undergo death to eliminate this niche for parasite replication. NLRP1 and NLRP3 have both been shown to recognize *T. gondii*[25-27] and could be the potential sensors in

414 microglia. AIM2 is another inflammasome sensor that can recognize DNA[63] and could therefore
415 be activated if parasite DNA becomes exposed to the cytosol. However, we and others[7] have not
416 been able to observe direct infection of microglia in chronically infected mice. On the other hand,
417 microglia migrate to sites of parasite reactivation and may recognize products resulting from host
418 cell death or damage, such as ATP, and undergo death that will promote inflammation. The
419 presence of ASC specks in infected brains suggests the formation of caspase-1-dependent
420 canonical inflammasome, but it remains unclear if the ASC specks are directly linked to IL-1α
421 release in microglia. Moreover, the canonical inflammasome can even be activated downstream of
422 non-canonical inflammasome driven gasdermin-D pores.[64] Thus, the sensors upstream of caspase-
423 dependent cleavage of gasdermin-D in microglia are of great interest.
424
425 **METHODS**
426
427 *Mice and infections*
428
429 C57BL/6 mice were purchased from The Jackson Laboratory or bred within our animal facility in
430 specific pathogen-free facilities. All mice were age- and sex-matched for all experiments.
431 Infections used the type II *T. gondii* strain Me49, which was maintained in chronically infected
432 Swiss Webster mice (Charles River Laboratories) and passaged through CBA/J mice (The Jackson
433 Laboratory) for experimental infections. For the experimental infections, the brains of chronically
434 infected (4-8 week) CBA/J mice were homogenized to isolate tissue cysts. Experimental mice were
435 then injected i.p. with 10 Me49 cysts. All procedures followed the regulations of the Institutional
436 Animal Care and Use Committee at the University of Virginia.

437

438 *Sampling*

439

440 Within a single experiment, when multiple parameters were assessed in the same tissue, the same
441 samples were used (i.e. for analysis of multiple immune cell populations by flow cytometry, cells
442 from the same brain sample were used). Representative IHC images accompanying flow cytometry
443 data were taken from distinct brain samples.

444

445 T. gondii *cyst counts*

446

447 Brain tissue was placed in complete RPMI, minced with a razor blade, and then passed through an
448 18-gauge needle. 30 µL of homogenate was placed on a microscope slide and covered with a
449 coverslip. Cysts were counted manually on a brightfield DM 2000 LED microscope (Leica
450 Biosystems).

451

452 *Tissue processing*

453

454 Immediately after sacrifice mice were perfused with 30 mL of cold 1X PBS. Brains and spleens
455 were harvested and put into cold complete RPMI media (cRPMI) (10% FBS, 1%
456 penicillin/streptomycin, 1% sodium pyruvate, 1% non-essential amino acids, and 0.1% 2-ME). If
457 peritoneal lavage fluid was collected, prior to perfusion, 5 mL of cold 1X PBS was injected through
458 the intact peritoneal membrane with a 26-gauge needle, and removed with a 22-gauge needle. If

serum was collected, blood from the heart was collected and allowed to clot at 4°C overnight to separate serum.

After harvest, brains were minced with a razor blade, passed through an 18-gauge needle, and then enzymatically digested with 0.227 mg/mL collagenase/dispase and 50 U/mL DNase (Roche) at 37°C for 45 minutes. After digestion, brains homogenate was passed through a 70 μm filter (Corning) and washed with cRPMI. To remove myelin from samples, filtered brain homogenate was then resuspended with 20 mL of 40% Percoll and spun at 650 x g for 25 minutes. Myelin was aspirated, samples were washed with cRPMI, and then resuspended in cRPMI. Spleens were mechanically homogenized and passed through a 40 μm filter (Corning). Samples were washed with cRPMI and then resuspended in 2 mL of RBC lysis buffer (0.16 M NH_4Cl) for 2 minutes. Cells were then washed with cRPMI and then resuspended. Peritoneal lavage fluid was washed with cRPMI, pelleted and resuspended.

Cytospin

Peritoneal lavage fluid samples were diluted to 1 x 10^5 cells/200 μL which was added to the upper chamber of the slide attachment (Simport). Samples were spun onto slides using a Cytospin 4 (Thermo Scientific), and then H&E stained.

Flow Cytometry and Cell Sorting

Single cell suspensions from tissue samples were plated in a 96-well U-bottom plate. Cells were initially incubated with 50 μL Fc block (1 μg/mL 2.4G2 Ab (BioXCell), 0.1% rat γ globulin

(Jackson ImmunoResearch)) for 10 minutes at room temperature. Cells were then surface stained with antibodies and a Live/Dead stain for 30 minutes at 4°C. After surface staining, cells were washed with FACS buffer (0.2% BSA and 2 mM EDTA in 1X PBS) and fixed at 4°C for 30 minutes with either 2% paraformaldehyde (PFA) or a fixation/permeabilization kit (eBioscience). Cells were then permeabilized and stained with any intracellular markers for 30 minutes at 4°C. Samples were then washed, resuspended in FACS buffer, and run on a Gallios flow cytometry (Beckman Coulter). Analysis was done using FlowJo software v.10. Antibody clones used include: CD31 (390), CD45 (30-F11), MHC-II (M5/114.15.2), NK1.1 (PK136), CD19 (1D3), CD3 (17A2), CD4 (GK1.5), CD11c (N418), CD11b (M1/70), Foxp3 (FJK-16s), Ly6G (1A8), Ly6C (HK1.4), CD8a (53-6.7), IFN-γ (XMG1.2), NOS2 (CXNFT), IL-1α (ALF-161), and pro-IL-1β (NJTEN3).

For cell sorting, CX3CR1cre^{ERT2} x ZsGreen$^{fl/stop/fl}$ mice were used. After surface staining, live cells were analyzed on a BD Aria in the UVA flow cytometry core facility. Cells were sorted based on ZsGreen expression, into serum-containing media for *ex vivo* culture, or into Trizol for RNA-sequencing.

ex vivo Culture Experiments

To assess IL-1 release, brain single-cell suspensions were plated in a 96-well plate in complete RPMI media with no additional stimulation. They were then incubated at 37°C for 4 hr to overnight (indicated in figure legends). For gasdermin-D inhibition assays, 20μM necrosulfonamide (NSA) was added to wells during incubation. Cells were pelleted and supernatants were collected for analysis. For sorted cell populations, equal numbers of microglia and macrophages were plated for analysis.

505

506 *Quantitative RT-PCR*

507

508 Approximately ¼ of a mouse brain was put into 1mL TRIzol (Ambion) in bead-beating tubes
509 (Sarstedt) containing 1 mm zirconia/silica beads (BioSpec). Tissue was homogenized for 30
510 seconds using a Mini-bead beater (BioSpec). RNA was extracted according to the manufacturer's
511 instructions (Ambion). High Capacity Reverse Transcription Kit (Applied Biosystems) was used
512 for cDNA synthesis. qRT-PCR was done using 2X Taq-based Master Mix (Bioline) and TaqMan
513 gene expression assays (Applied Biosystems). Reactions were run on a CFX384 Real-Time
514 System (Bio-Rad Laboratories). HPRT was used as the housekeeping gene for all reactions and
515 relative expression was calculated as $2^{(-\Delta\Delta CT)}$.

516

517 *Immunohistochemistry*

518

519 Brains from mice were harvested and placed in 4% PFA for 24 hours. Following PFA fixation,
520 brains were moved to a solution of 30% sucrose for 24 hours, and were then embedded in OCT
521 and flash frozen on dry ice. Samples were stored at -20°C until cutting. After cutting, sections were
522 blocked in 1X PBS containing 0.1% triton, 0.05% Tween 20, and 2% goat or donkey serum
523 (Jackson ImmunoResearch) for 1 hour at room temperature. Sections were then incubated with
524 primary Abs overnight at 4°C. Sections were then washed with PBS, and incubated with secondary
525 Abs for 1 hour at room temperature. Sections were then washed, and nuclear stained with DAPI
526 (Thermo Fisher Scientific) for 5 minutes at room temperature. Finally, sections were mounted,
527 covered in Aquamount (Lerner Laboratories), and covered with coverslips (Thermo Fisher

Scientific). All images were captured using a Leica TCS SP8 Confocal microscopy system. Images were analyzed using either ImageJ or Imaris software.

H&E Tissue Sections

Brains from mice were submerged in formalin and sent to the UVA Research Histology Core, where they were embedded in paraffin and sectioned. They were then imaged on on a brightfield DM 2000 LED microscope (Leica Biosystems).

ELISAs

Samples for ELISAs were obtained by harvesting mouse brains and processing them to form a single cell suspension. Cells were then plated in 96-well plates and incubated at 37°C either overnight or for 5 hours (indicated in figure legends). Supernatants were then collected and stored at -20°C until use. ELISAs for IL-1α and IL-1β (BioLegend), as well as for IFN-γ, were performed according to the manufacturer's instructions. Briefly, Immunolon 4HBX ELISA plates (Thermo Fisher Scientific) were coated with capture antibody at 4° overnight. Plates were then washed and blocked with buffer containing BSA at room temperature for 1 hour. After washing, standards and samples were added and incubated at room temperature for 2 hours. After washing, biotinylated detection antibody was added and incubated for 1 hour at room temperature. Plates were washed and incubated with avidin-HRP for 30 minutes at room temperature. Finally, plates were washed and incubated with ABTS peroxide substrate solution (SouthernBiotech) for 15 minutes or until

color change occurred. Immediately after color change, plates were read on an Epoch Biotek plate reader using Gen5 2.00 software.

Ab Blockade Experiments

Chronically infected mice (4 weeks p.i.) were treated on days 1 and 3 of the treatment regimen with 200 µg i.p. each of anti-LFA-1 and anti-VLA-4 blocking antibodies (Bio X Cell) or control IgG. They were then sacrificed and analyzed on day 5.

Propidium Iodide Injection

Chronically infected mice (4 weeks p.i.) were injected i.p. with 0.4 mg of propidium iodide. 24 hours after injection, mice were sacrificed and their brains were PFA fixed and analyzed by confocal microscopy.

Microglia Depletion

For studies involving microglia depletion, mice were fed either control chow or chow containing PLX5622 *ad libitum* for 12 days prior to harvest.

Bone Marrow Chimeras

At 8 weeks of age, C57B6/J and *Il1r1*$^{-/-}$ mice were irradiated with 1000 rad. Bone marrow cells isolated from WT and *Il1r1*$^{-/-}$ mice were then i.v. transferred (by retro-orbital injection) into the irradiated recipient mice. Mice were allowed to recover for 6 weeks after irradiation and

572 reconstitution and were then infected. 4 weeks post infection, mice were sacrificed and tissues
573 were harvested for analysis.
574
575 *RNA Sequencing Data Analysis*
576
577 Pre-Processing/Primary Analysis:
578 Read quality profiles for raw FASTQ files was performed with FastQC (v0.11.5) before and after
579 trimming and filtering. Read filtering and trimming was accomplished with Trimmomatic (v0.39)
580 paired-end set to phred33 quality scoring. Reads were trimmed according to a four-base sliding
581 window with a minimum quality score of 15 and minimum leading and trialing quality scores of
582 3. The minimum fragment length was set to 36. Trimmed and filtered reads were mapped to the
583 GENCODE M13 genome and transcript abundances were quantified using Salmon (v0.8.2).
584 Quantified transcript abundances were imported into the R programming environment and
585 converted into ENSEMBL gene abundances with Tximport (v1.4.0). All pre-processing steps were
586 performed within the Pypiper framework (v0.6.0) with Python version 2.7.14.
587 Secondary and Tertiary Analysis:
588 Differential expression testing was performed using the R Bioconductor package DESeq2
589 (v1.16.1) at a preset alpha value of 0.05. Log2 fold change values were shrunken using a normal
590 prior distribution. Any results that lacked the replicates or had low counts were thrown out of the
591 dataset prior to differential expression testing. Results of differential expression testing were
592 visualized using the R package EnhancedVolcano (v1.2.0) to display transformed p-values (-
593 log10) against the corresponding log2 fold change values. All labeled genes were manually
594 selected from significantly differentially expressed genes in the DESeq2 results list.

595 Differential expression testing results were labeled as "upregulated" or downregulated" for
596 a given pairwise comparison. All genes with a log2 fold change value above 0 and a BH adjusted
597 p-value below 0.05 were designated upregulated and all genes with a log2 fold change value below
598 0 and a BH adjusted p-value below 0.05 were designated downregulated. Gene names for the
599 differential expression results tables were converted from mouse ENSEMBL codes to gene
600 symbols with AnnotationDbi (v1.46.0). In order to determine the functional profile of the gene
601 lists, the R package clusterProfiler (v3.12.0) was used to apply Fisher's exact test with respect to
602 over-representation of GO terms for biological processes at all levels of the Gene Ontology
603 Consortium hierarchy. The lists were tested against a background distribution that consisted of all
604 genes that returned a p-value in differential expression testing. Significant GO terms had a BH
605 adjusted p-value below 0.05.
606 GO terms were manually selected from the results output in the clusterProfiler package for
607 plotting with the pheatmap package (v1.0.12). Each GO term-specific heatmap displays rlog-
608 transformed abundance values that have been Z-score normalized with respect to each gene. The
609 genes displayed were selected from clusterProfiler results for enrichment of GO terms for
610 biological processes. Significantly enriched GO terms were also selected and plotted using the
611 clusterProfiler dotplot function.
612
613 *Statistics*
614
615 Statistical analysis comparing two groups at a single time point was performed in Prism software
616 using an unpaired Student's T test. When data from multiple experiments were combined, to show
617 natural biological variability between infections, a randomized block ANOVA was performed

using R v.3.4.4 software. This test was designed to assess the effect of experimental group while controlling for any effect of experimental date, by modeling the group as a fixed effect and date as a random effect. Tests used for each figure is shown in the figure legend. All data were graphed using Prism software. Distributions were assumed to be normal. All graphs show the mean of the data, or the mean along with individual values. Error bars indicate standard deviation.

ACKNOWLEDGEMENTS

The authors would like to acknowledge members of the Harris lab and center for Brain Immunology and Glia (BIG) for their input during the development of this work. We thank Marieke K. Jones for her help with statistical analysis and coding. We thank Sarah Ewald and her lab at UVA for sharing the ASC-citrine mice used in this study. We would like to acknowledge the support we received from core facilities at the University of Virginia, including the Flow Cytometry Core and the Research Histology Core.

AUTHOR CONTRIBUTIONS

S.J.B. designed and performed experiments, analyzed data, and wrote the manuscript. K.M.S. and C.A.O. helped with experiments and discussed results and implications. J.A.T. performed the RNA-seq experiment. D.J. conducted bioinformatics analyses. J.R.L. provided reagents, mice, and conceptual advice. T.H.H. supervised the project and edited the manuscript.

COMPETING INTERESTS STATEMENT

The authors declare no competing interest.

FIGURE LEGENDS

Figure 1. Microglia and macrophages in the infected brain differ in inflammatory signature and IL-1 expression

a-d, Chronically infected $CX_3CR_1^{Cre\text{-}ERT2}$ x $ZsGreen^{fl/stop/fl}$ mice were sacrificed and brains were harvested and processed for flow cytometry (n = 4 mice). Samples were run on a BD Aria, gated on live/singlets/$CD45^+$/$CD11b^+$ from which $ZsGreen^+$ and $ZsGreen^-$ populations were gated and sorted. Sorted cell populations were subjected to RNA sequencing. **a,** Experimental setup. **b,** Differential abundance testing was performed and results were plotted in R to produce a volcano plot showing differentially expressed genes between microglia and macrophage populations. Example genes are labeled in red corresponding to green dots. **c,** GO terms statistically over-represented in macrophages compared to microglia were generated and a selection of significantly enriched pathways of interest were plotted using R. **d,** Significantly differentially expressed genes between the two cell populations were selected based on interest and plotted in a heatmap using complete-linkage clustering of a euclidean distance matrix of all samples. **e-l,** Representative images of brain sections from chronically infected $CX_3CR_1^{Cre\text{-}ERT2}$ x $ZsGreen^{fl/stop/fl}$ mice. ZsGreen is shown in green (**e-f,j,l**) and sections were stained for Iba1 (green, **g-h**; gray, **i,k**), RelA (**e,g** red), Rel (**f,h** red), IL-1β (**i-j** red), and IL-1α (**k-l** red). Scale bars indicate 30 μm.

Figure 2. IL-$1R^{-/-}$ mice have an impaired immune response to *T. gondii* infection.

WT C57B6/J or *Il1r1*$^{-/-}$ mice were infected i.p. with 10 cysts of the Me49 strain of *T. gondii*. 6 weeks p.i. brains were harvested and homogenized. (n = 3-5 mice per group per experiment) **a,** Cyst burden per brain was determined by counting cysts in brain homogenate on a light microscope. Paired averages from 5 experiments are shown, and statistics were performed using a

randomized block ANOVA. **b-g,** Brains from the same mice were processed to achieve a single cell suspension and analyzed by flow cytometry. Data compiled from 4 experiments; statistics were performed using a randomized block ANOVA. **b,** Blood derived myeloid cells were defined as $CD11b^{+}CD45^{hi}$, cells were pre-gated on singlets/live/$CD45^{+}$/$CD11c^{-}$, representative flow plots are shown in (**f-g**). **c,** The number of $iNOS^{+}$ cells per brain were calculated, pre-gated on singlets/live/$CD45^{+}$/$CD11c^{-}$/$CD11b^{+}CD45^{hi}$, representative flow plots are shown in (**h-i**). **d-e,** $CD8^{+}$ and $CD4^{+}$ T cell numbers were calculated, pre-gated on singlets/live/$CD3^{+}$. **j-k,** Representative confocal images of focal areas of inflammation in chronically infected brains of WT (**j**) and IL-1r1$^{-/-}$ (**k**) mice. * = $p < 0.05$, ** = $p < 0.01$, *** = $p < 0.001$. Scale bars indicate 50 μm.

Figure 3. IL-1R1 is expressed on brain vasculature during chronic *T. gondii* infection.

a-b, Brains from chronically infected C57B6/J WT mice were sectioned and stained with DAPI (blue) and antibodies against laminin (red) and IL-1r1 (green), showing parenchymal blood vessels. **c-e,** WT (CD45.1) and *Il1r1*$^{-/-}$ (CD45.2) mice were lethally irradiated and then reconstituted with bone marrow from either WT or *Il1r1*$^{-/-}$ mice. Mice were allowed to reconstitute for 6 weeks and then were infected i.p. with 10 cysts of the Me49 strain of *T. gondii*. 4 weeks p.i. mice were sacrificed and their brains were harvested for analysis. (n = 3-6 mice per group per experiment) **d,** Brains were homogenized and cysts were counted by light microscopy. **e,** Brains were processed for flow cytometry and the numbers of total leukocytes were calculated. Cells were pre-gated on singlets/live. **d-e,** Data compiled from 2 experiments, statistics performed using a randomized block ANOVA. **f,** WT and *Ilr1*$^{-/-}$ mice were infected i.p. with 10 cysts of the Me49 strain of *T. gondii*. 6 weeks p.i. the mice were sacrificed and brains were homogenized, RNA was

extracted, and qPCR analysis was performed. Data compiled from 2 (CCL2) or 3 (ICAM1, VCAM1) experiments; statistics performed using a randomized block ANOVA. (n = 3-5 mice per group per experiment) **g-j,** Brains from chronically infected WT and *Il1r1*$^{-/-}$ mice were sectioned and stained for either ICAM-1 (**g-h**) or VCAM-1 (**i-j**). Representative images of blood vessels are shown. **g-h,** scale bars are 50 μm and (**i-j**) scale bars are 60 μm. * = $p < 0.05$, ** = $p < 0.01$, *** = $p < 0.001$.

Figure 4. IL-1α$^{-/-}$ but not IL-1β$^{-/-}$ mice have an impaired response to *T. gondii* infection.

WT C57B6/J, IL-1α$^{-/-}$, and IL-1β$^{-/-}$were infected i.p. with 10 cysts of the Me49 strain of *T. gondii*. 6 weeks p.i. brains were harvested and analyzed. **a,** Genomic DNA was isolated from brain homogenate, and parasite DNA was quantified using real-time qPCR. Data compiled from 2 experiments; statistics performed using a randomized block ANOVA. (n = 3-4 mice per group per experiment) **b-c,** Brain slices from WT (**b**) and IL-1α$^{-/-}$ (**c**) were H&E stained and representative images are shown. Arrow heads indicate clusters of immune cells. **d-k,** Brains were processed to obtain a single cell suspension, and analyzed by flow cytometry. Paired averages from 4 or 5 compiled experiments, statistics performed using a randomized block ANOVA. (n = 3-5 mice per group per experiment) **d,h,** Blood-derived myeloid cells per brain as defined by CD11b^{+}CD45^{hi}. Cells were pre-gated on singlets/live/CD45^{+}/CD11c^{-}. **e,i,** iNOS^{+} cells per brain were quantified, pre-gated on singlets/live/CD45^{+}/CD11c^{-}/CD11b^{+}CD45^{hi}. **f-g, j-k,** CD8^{+} and CD4^{+} T cells were quantified, pre-gated on singlets/live/CD3^{+}. * = $p < 0.05$, ** = $p < 0.01$, *** = $p < 0.001$.

Figure 5. IL-1α is released *ex vivo* from microglia from *T. gondii* infected brains.

a, Uninfected mice were fed either control chow or chow containing PLX5622 for 12 days prior to sacrifice. mRNA levels of IL-1α were determined by RT-qPCR on whole brain homogenate. (n = 2 mice per group) **b,** 6 weeks p.i. brains from WT mice were harvested and processed to a single cell suspension. Cells were plated in a 96 well plate and incubated at 37°C overnight. IL-1α release was then measured by ELISA. (n = 3 mice per group) **c-d,** Chronically infected $CX_3CR_1^{Cre\text{-}ERT2}$ x $ZsGreen^{fl/stop/fl}$ mice were sacrificed and brains were harvested and processed for flow cytometry. Samples were run on a BD Aria, gated on live/singlets/$CD45^+$/$CD11b^+$ from which $ZsGreen^+$ and $ZsGreen^-$ populations were gated and sorted. Cells from 6 mice were pooled. Equal numbers of each cell population were plated and incubated overnight at 37°C. (n = 3-4 wells per group) Supernatants were collected and analyzed by ELISA for IL-1α (**c**) and LDH (**d**) (plotted as absorbance at 490nm-680nm). For (**c**) results from two experiments are shown. **e-f,** Assay was performed as in **b**, with some wells treated with glycine to stop membrane permeability (**e**) or triton-containing lysis buffer to show total possible release (**f**). Statistics were performed using Student's T test (**a-b, d-e**) or a Randomized Block ANOVA (**c**). * = $p < 0.05$, ** = $p < 0.01$, *** = $p < 0.001$.

Figure 6. Caspase-$1/11^{-/-}$ mice have an impaired response to *T. gondii* infection.

a-b, Chronically infected C57B6/J mice were injected i.p. with 20 mg/kg propidium iodide. 24 hrs later, mice were sacrificed and brains were imaged with confocal microscopy. A representative image is shown. **c-d,** Mice expressing ASC-citrine (**c**) or ASC-citrine and CX3CR1-cre^{ERT2}ZsGreen (**d**) were infected with 10 cysts of the Me49 strain of *T. gondii*. 4 weeks post infection brains were harvested, cryopreserved, stained, and imaged. Arrows indicate ASC aggregates in $Iba1^+$ cells (**c**) or in $ZsGreen^+$ microglial cells (**d**). **e-i,** WT and casp-$1/11^{-/-}$ mice were

732 infected with 10 cysts of the Me49 strain of *T. gondii*. 6 weeks p.i. brains were harvested and
733 analyzed. Paired averages for 3-6 experiments are shown. (n = 3-5 mice per group per experiment)
734 (**e**) Cyst burden per brain was determined by counting cysts in brain homogenate on a light
735 microscope. **f,** Infiltrating myeloid cell populations were quantified by flow cytometry. Cells were
736 pre-gated on singlets/live/$CD45^+$/$CD11c^-$. **g,** $iNOS^+$ cell populations were quantified, cells were
737 pre-gated on singlets/live/$CD45^+$/$CD11c^-$/$CD11b^+$/$CD45^{hi}$. **h-i,** $CD8^+$ and $CD4^+$ T cell populations
738 were quantified, cells were pre-gated on live/singlets/$CD3^+$. **j-k,** Brain slices from WT (**j**) and
739 caspase-$1/11^{-/-}$ (**k**) mice were H&E stained and representative images are shown. Arrow heads
740 indicate parasite cysts. Statistics were performed using a randomized block ANOVA (**e-i**). * = $p < 0.05$, ** = $p < 0.01$, *** = $p < 0.001$. Scale bars in (**a-b**) are 400 μm, scale bar in (**d**) is 15 μm,
742 all other scale bars are 50 μm.
743
744 **Figure 7. Gasdermin $D^{-/-}$ mice have an impaired response to *T. gondii* infection and impaired**
745 **IL-1α release.**
746 **a-c,** C57B6/J and Gasdermin $D^{-/-}$ mice were infected i.p. with 10 cysts of the Me49 strain of *T.*
747 *gondii*. 6 weeks p.i., mice were sacrificed and tissues were harvested for analysis. Data from two
748 experiments are shown (n = 4-5 mice per group) **a,** Cyst burden per brain was determined by
749 counting cysts in brain homogenate on a light microscope. **b,** Brain tissue was processed for flow
750 cytometry analysis and immune cell populations were quantified. All populations were previously
751 gated on live/singlets. $CD4^+$ and $CD8^+$ were pre-gated on $CD3^+$ T cells; DCs were pre-gated on
752 $CD45^+$ cells; infiltrating macrophage/monocytes (Mϕ) are defined as $CD11c^-CD11b^+CD45^{hi}$;
753 $iNOS^+$ cells were gated within the Mϕ gate. **c,** Single cell suspension from brain homogenate from
754 WT and $Gsdmd^{-/-}$ mice was plated in a 96 well plate and incubated at 37°C overnight. Supernatant

755 was isolated and analyzed by ELISA for IL-1α. **d,** Brain homogenate from WT mice was plated
756 as in **c**, with either control media or 20 μm necrosulfonamide (NSA). IL-1α release from two
757 experiments is shown (**d**). (n = 4 wells per group per experiment) Statistics were performed using
758 a randomized block ANOVA. * = $p < 0.05$, ** = $p < 0.01$, *** = $p < 0.001$.
759
760 **Supplementary Figure 1. Microglia and macrophages in the infected brain differ in IL-1**
761 **expression.**
762 **a-d,** $CX_3CR_1^{Cre\text{-}ERT2}$ x $ZsGreen^{fl/stop/fl}$ mice were left naïve or infected with 10 cysts of Me49 strain
763 *T. gondii* parasites for 4 weeks. (n = 4 mice per group) **a,** Representative image of IL-1α in naïve
764 brain colocalizing with microglia, scale bar is 50 μm. **b-d,** Brains were harvested and analyzed by
765 flow cytometry with intracellular cytokine staining. Numbers of IL-1α$^+$ (**b**), IL-1β$^+$ (**c**), and double
766 positive (**d**) cells were quantified in both ZsGreen$^+$ and ZsGreen$^-$ populations in naïve and infected
767 mice. Cells were pre-gated on singlets/live/ZsGreen. **e-g,** Brains from naïve or chronically infected
768 mice were analyzed by flow cytometry. **e,** Representative plots of IL-1α expression for naïve
769 samples, previously gated on live/singlets. **f-g,** Representative plots of IL-1α (**f**) and IL-1β (**g**)
770 expression for infected samples.
771
772 **Supplementary Figure 2. Brain IFN-γ responses and peripheral immune responses are not**
773 **impaired in *Il1r1*$^{-/-}$ mice during chronic *T. gondii* infection.**
774 WT and *Il1r1*$^{-/-}$ mice were infected i.p. with 10 cysts of the Me49 strain of *T. gondii*. 6 weeks p.i.
775 brains (**a-b)** and spleens (**c-h**) were harvested and processed for flow cytometry. Immune cell
776 populations were enumerated. **a-b,** Brains were harvested and digested. Isolated cells were
777 incubated at 37°C for 5 hours with a mix of PMA/ionomycin and brefeldin A. Intracellular

cytokine staining was performed and analyzed by flow cytometry. Cells were pre-gated on singlets/Live/$CD3^+$ and percent (**a**) and number (**b**) of IFN-γ^+ CD4 and $CD8^+$ T cells were determined. **c,** Total immune cells, pre-gated on singlets/live. **d,** DCs, pre-gated on singlets/live/$CD45^+$/$Dump^-$(CD3/NK1.1/B220). **e,** Monocytes/ macrophages, pre-gated on singlets/live/ $CD45^+$/$CD11c^-$/$CD11b^+$/$CD45^{hi}$. **f,** $CD8^+$ T cells, pre-gated on singlets/live/$CD3^+$. **g,** Effector $CD4^+$ T cells, pre-gated on singlets/live/$CD3^+$. **h,** Tregs, pre-gated on singlets/live/$CD3^+$. **a-b,** A representative experiment is shown and statistics were performed using a Student's T test. (n = 4-5 mice per group) **c-h,** Paired averages compiled from 3-6 experiments. Statistics were performed using a randomized block ANOVA. (n = 3-5 mice per group per experiment) * = $p < 0.05$, ** = $p < 0.01$, *** = $p < 0.001$.

Supplementary Figure 3. IFN-γ response and monocyte/macrophage response during acute infection are not impaired in *Il1r1*$^{-/-}$ mice.

WT and *Il1r1*$^{-/-}$ mice were infected i.p. with 10 cysts of the Me49 strain of *T. gondii*. Mice were sacrificed 12 days p.i. **a,** Peritoneal lavage was performed and peritoneal exudate cells (PECs) were isolated and analyzed by flow cytometry. **b,** Spleen cells were isolated and analyzed by flow cytometry. **c,** Serum was harvested at the time of sacrifice and IFN-γ in the serum was analyzed by ELISA. A representative experiment is shown (n = 4 mice per group). Statistics were performed using a Student's t-test between groups for each measure.

Supplementary Figure 4. IL-1R1 is expressed by endothelial cells in the brain.

a, Brains from chronically infected C57B6/J mice were harvested, fixed, and stained with antibodies against CD31 (red) and IL-1R1 (green). **b-c,** Brains from uninfected C57B6/J mice

were harvested and processed for flow cytometry analysis. Cells were previously gated on Singlets/Live/CD45$^-$ and then were gated on CD31$^+$ (**b**) and IL-1R1 (**c**) expression on the CD31$^+$ population.

Supplementary Figure 5. The brain endothelium is activated during chronic *T. gondii* infection.

a-d, WT C57B6/J mice were either left naïve or infected i.p. with the Me49 strain of *T. gondii*. 4 weeks p.i. mice were sacrificed and brains were harvested for flow cytometry analysis. (n = 2 mice per group) **a-b,** Samples were pre-gated on singlets/live/Hoescht$^+$/CD45$^-$/CD31$^+$ and then ICAM-1 expression was assessed. Representative plots from naïve (**a**) and infected (**b**) mice are shown. **c-d,** Samples were pre-gated as in **a** and then VCAM-1 expression was assessed. Representative plots from naïve (**c**) and infected (**d**) mice are shown. **e,** Histogram showing ICAM-1 expression on IL-1R1 positive and negative endothelial cells, the FMO is shown in filled gray **f,** Brains from chronically infected C57B6/J mice were harvested, fixed, and stained with antibodies against laminin (gray), IL-1r1 (red), and VCAM-1 (green). **g-i,** C57B6/J mice were infected i.p. with 10 cysts of the Me49 strain of *T. gondii*. 4 weeks p.i. mice were treated with either control IgG or 200 μg each of α-LFA-1 and α-VLA-4 blocking antibodies on days 1 and 3 of treatment, and were sacrificed on day 5. Brains were harvested and processed for flow cytometry. (n = 4-5 mice per group) **g,** Cells were previously gated on singlets/live/CD11c$^-$/CD45$^+$ and the numbers of CD11b$^+$CD45^{hi} cells are shown. Of the CD45^{hi} cells numbers of Ly6C^{hi} cells (**h**) and iNOS$^+$ cells (**i**) were enumerated. Statistics were performed using a Student's T-test. * = $p < 0.05$ ** = $p < 0.01$, *** = $p < 0.001$.

Supplementary Figure 6. Example gating strategy for brain immune populations.

Myeloid and T cell populations were identified using two separate panels. **a-b,** for all panels, samples were first gated on singlets and then cells which excluded the live/dead dye. **c-e,** to identify T cell populations, live cells were plotted to gate on either CD8+CD3+ (**c**) or CD4+CD3+ (**d**) cells. **e,** to identify Tregs, CD4+ T cells were gated on Foxp3+. **f-j,** to identify myeloid cell populations live cells were first gated on CD45+ (**f**). CD45+ cells were then gated on CD11c and MHCII (**g**), CD11c+MHCII hi cells were called DCs. CD11c- cells were then gated by CD45 and CD11b (**i**). CD11b+CD45int cells were called microglia, and CD11b+CD45hi cells were called infiltrating myeloid cells. CD45hi cells were then gated on iNOS+ (**j**).

REFERENCES

1 Pappas, G., Roussos, N. & Falagas, M. E. Toxoplasmosis snapshots: global status of Toxoplasma gondii seroprevalence and implications for pregnancy and congenital toxoplasmosis. *Int J Parasitol* **39**, 1385-1394, doi:10.1016/j.ijpara.2009.04.003 (2009).

2 Belanger, F., Derouin, F., Grangeot-Keros, L. & Meyer, L. Incidence and risk factors of toxoplasmosis in a cohort of human immunodeficiency virus-infected patients: 1988-1995. HEMOCO and SEROCO Study Groups. *Clin Infect Dis* **28**, 575-581, doi:10.1086/515147 (1999).

3 Flegr, J., Prandota, J., Sovickova, M. & Israili, Z. H. Toxoplasmosis--a global threat. Correlation of latent toxoplasmosis with specific disease burden in a set of 88 countries. *PLoS One* **9**, e90203, doi:10.1371/journal.pone.0090203 (2014).

4 Jones, J. L. *et al.* Toxoplasma gondii infection in the United States: seroprevalence and risk factors. *Am J Epidemiol* **154**, 357-365 (2001).

5 Luft, B. J. & Remington, J. S. Toxoplasmic encephalitis in AIDS. *Clin Infect Dis* **15**, 211-222 (1992).

6 Renold, C. *et al.* Toxoplasma encephalitis in patients with the acquired immunodeficiency syndrome. *Medicine (Baltimore)* **71**, 224-239 (1992).

7 Cabral, C. M. *et al.* Neurons are the Primary Target Cell for the Brain-Tropic Intracellular Parasite Toxoplasma gondii. *PLoS Pathog* **12**, e1005447, doi:10.1371/journal.ppat.1005447 (2016).

8 Dubey, J. P. Bradyzoite-induced murine toxoplasmosis: stage conversion, pathogenesis, and tissue cyst formation in mice fed bradyzoites of different strains of Toxoplasma gondii. *J Eukaryot Microbiol* **44**, 592-602 (1997).

9 Brown, C. R. & McLeod, R. Class I MHC genes and CD8+ T cells determine cyst number in Toxoplasma gondii infection. *J Immunol* **145**, 3438-3441 (1990).

10 Gazzinelli, R., Xu, Y., Hieny, S., Cheever, A. & Sher, A. Simultaneous depletion of CD4+ and CD8+ T lymphocytes is required to reactivate chronic infection with Toxoplasma gondii. *J Immunol* **149**, 175-180 (1992).

11 Gazzinelli, R. T., Hakim, F. T., Hieny, S., Shearer, G. M. & Sher, A. Synergistic role of CD4+ and CD8+ T lymphocytes in IFN-gamma production and protective immunity induced by an attenuated Toxoplasma gondii vaccine. *J Immunol* **146**, 286-292 (1991).

12 Pfefferkorn, E. R. Interferon gamma blocks the growth of Toxoplasma gondii in human fibroblasts by inducing the host cells to degrade tryptophan. *Proc Natl Acad Sci U S A* **81**, 908-912 (1984).

13 Nathan, C. F., Murray, H. W., Wiebe, M. E. & Rubin, B. Y. Identification of interferon-gamma as the lymphokine that activates human macrophage oxidative metabolism and antimicrobial activity. *J Exp Med* **158**, 670-689 (1983).

14 Selleck, E. M. *et al.* Guanylate-binding protein 1 (Gbp1) contributes to cell-autonomous immunity against Toxoplasma gondii. *PLoS Pathog* **9**, e1003320, doi:10.1371/journal.ppat.1003320 (2013).

15 Murray, H. W., Spitalny, G. L. & Nathan, C. F. Activation of mouse peritoneal macrophages in vitro and in vivo by interferon-gamma. *J Immunol* **134**, 1619-1622 (1985).

16 Ling, Y. M. *et al.* Vacuolar and plasma membrane stripping and autophagic elimination of Toxoplasma gondii in primed effector macrophages. *J Exp Med* **203**, 2063-2071, doi:10.1084/jem.20061318 (2006).

17 Degrandi, D. *et al.* Murine guanylate binding protein 2 (mGBP2) controls Toxoplasma gondii replication. *Proc Natl Acad Sci U S A* **110**, 294-299, doi:10.1073/pnas.1205635110 (2013).

18 Biswas, A. *et al.* Ly6C(high) monocytes control cerebral toxoplasmosis. *J Immunol* **194**, 3223-3235, doi:10.4049/jimmunol.1402037 (2015).

19 Kim, B. *et al.* The Interleukin-1alpha Precursor is Biologically Active and is Likely a Key Alarmin in the IL-1 Family of Cytokines. *Front Immunol* **4**, 391, doi:10.3389/fimmu.2013.00391 (2013).

20 Di Paolo, N. C. & Shayakhmetov, D. M. Interleukin 1alpha and the inflammatory process. *Nat Immunol* **17**, 906-913, doi:10.1038/ni.3503 (2016).

21 Black, R. A. *et al.* Generation of biologically active interleukin-1 beta by proteolytic cleavage of the inactive precursor. *J Biol Chem* **263**, 9437-9442 (1988).

22 Broz, P. & Dixit, V. M. Inflammasomes: mechanism of assembly, regulation and signalling. *Nat Rev Immunol* **16**, 407-420, doi:10.1038/nri.2016.58 (2016).

23 He, W. T. *et al.* Gasdermin D is an executor of pyroptosis and required for interleukin-1beta secretion. *Cell Res* **25**, 1285-1298, doi:10.1038/cr.2015.139 (2015).

24 Dower, S. K. *et al.* The cell surface receptors for interleukin-1 alpha and interleukin-1 beta are identical. *Nature* **324**, 266-268, doi:10.1038/324266a0 (1986).

25 Cirelli, K. M. *et al.* Inflammasome sensor NLRP1 controls rat macrophage susceptibility to Toxoplasma gondii. *PLoS Pathog* **10**, e1003927, doi:10.1371/journal.ppat.1003927 (2014).

26 Ewald, S. E., Chavarria-Smith, J. & Boothroyd, J. C. NLRP1 is an inflammasome sensor for Toxoplasma gondii. *Infect Immun* **82**, 460-468, doi:10.1128/IAI.01170-13 (2014).

27 Gorfu, G. *et al.* Dual role for inflammasome sensors NLRP1 and NLRP3 in murine resistance to Toxoplasma gondii. *MBio* **5**, doi:10.1128/mBio.01117-13 (2014).

28 Coutermarsh-Ott, S. L. *et al.* Caspase-11 Modulates Inflammation and Attenuates Toxoplasma gondii Pathogenesis. *Mediators Inflamm* **2016**, 9848263, doi:10.1155/2016/9848263 (2016).

29 Still, K. M. B., S.J.; Thompson, J.A.; Hayes, N.W.; O'Brien, C.; Harris, T.H. The damage signal IL-33 promotes a focal protective myeloid cell response to Toxplasma gondii in the brain. *bioRxiv*, doi:https://doi.org/10.1101/338400 (2018).

30 Yona, S. *et al.* Fate mapping reveals origins and dynamics of monocytes and tissue macrophages under homeostasis. *Immunity* **38**, 79-91, doi:10.1016/j.immuni.2012.12.001 (2013).

31 Sedgwick, J. D. *et al.* Isolation and direct characterization of resident microglial cells from the normal and inflamed central nervous system. *Proc Natl Acad Sci U S A* **88**, 7438-7442 (1991).

32 Martin-Sanchez, F. *et al.* Inflammasome-dependent IL-1beta release depends upon membrane permeabilisation. *Cell Death Differ* **23**, 1219-1231, doi:10.1038/cdd.2015.176 (2016).

33 Rubartelli, A., Cozzolino, F., Talio, M. & Sitia, R. A novel secretory pathway for interleukin-1 beta, a protein lacking a signal sequence. *EMBO J* **9**, 1503-1510 (1990).

34 Gross, O. *et al.* Inflammasome activators induce interleukin-1alpha secretion via distinct pathways with differential requirement for the protease function of caspase-1. *Immunity* **36**, 388-400, doi:10.1016/j.immuni.2012.01.018 (2012).

35 Chen, X. *et al.* Pyroptosis is driven by non-selective gasdermin-D pore and its morphology is different from MLKL channel-mediated necroptosis. *Cell Res* **26**, 1007-1020, doi:10.1038/cr.2016.100 (2016).

36 Liu, X. *et al.* Inflammasome-activated gasdermin D causes pyroptosis by forming membrane pores. *Nature* **535**, 153-158, doi:10.1038/nature18629 (2016).

37 Kanneganti, A. *et al.* GSDMD is critical for autoinflammatory pathology in a mouse model of Familial Mediterranean Fever. *J Exp Med* **215**, 1519-1529, doi:10.1084/jem.20172060 (2018).

38 Rathkey, J. K. *et al.* Chemical disruption of the pyroptotic pore-forming protein gasdermin D inhibits inflammatory cell death and sepsis. *Sci Immunol* **3**, doi:10.1126/sciimmunol.aat2738 (2018).

39 Blanchard, N., Dunay, I. R. & Schluter, D. Persistence of Toxoplasma gondii in the central nervous system: a fine-tuned balance between the parasite, the brain and the immune system. *Parasite Immunol* **37**, 150-158, doi:10.1111/pim.12173 (2015).

40 Chao, C. C. *et al.* Effects of cytokines on multiplication of Toxoplasma gondii in microglial cells. *J Immunol* **150**, 3404-3410 (1993).

41 Chao, C. C. *et al.* Activated microglia inhibit multiplication of Toxoplasma gondii via a nitric oxide mechanism. *Clin Immunol Immunopathol* **67**, 178-183, doi:10.1006/clin.1993.1062 (1993).

42 Chao, C. C., Gekker, G., Hu, S. & Peterson, P. K. Human microglial cell defense against Toxoplasma gondii. The role of cytokines. *J Immunol* **152**, 1246-1252 (1994).

43 Bohlen, C. J. *et al.* Diverse Requirements for Microglial Survival, Specification, and Function Revealed by Defined-Medium Cultures. *Neuron* **94**, 759-773 e758, doi:10.1016/j.neuron.2017.04.043 (2017).

44 Buttgereit, A. *et al.* Sall1 is a transcriptional regulator defining microglia identity and function. *Nat Immunol* **17**, 1397-1406, doi:10.1038/ni.3585 (2016).

45 Chatziandreou, N. *et al.* Macrophage Death following Influenza Vaccination Initiates the Inflammatory Response that Promotes Dendritic Cell Function in the Draining Lymph Node. *Cell Rep* **18**, 2427-2440, doi:10.1016/j.celrep.2017.02.026 (2017).

46 Rabolli, V. *et al.* The alarmin IL-1alpha is a master cytokine in acute lung inflammation induced by silica micro- and nanoparticles. *Part Fibre Toxicol* **11**, 69, doi:10.1186/s12989-014-0069-x (2014).

47 Benjamin, J. T. *et al.* Cutting Edge: IL-1alpha and Not IL-1beta Drives IL-1R1-Dependent Neonatal Murine Sepsis Lethality. *J Immunol* **201**, 2873-2878, doi:10.4049/jimmunol.1801089 (2018).

48 Bastien, D. *et al.* IL-1alpha Gene Deletion Protects Oligodendrocytes after Spinal Cord Injury through Upregulation of the Survival Factor Tox3. *J Neurosci* **35**, 10715-10730, doi:10.1523/JNEUROSCI.0498-15.2015 (2015).

49 Vanlandewijck, M. *et al.* A molecular atlas of cell types and zonation in the brain vasculature. *Nature* **554**, 475-480, doi:10.1038/nature25739 (2018).

50 Liu, X. *et al.* Cell-Type-Specific Interleukin 1 Receptor 1 Signaling in the Brain Regulates Distinct Neuroimmune Activities. *Immunity* **50**, 317-333 e316, doi:10.1016/j.immuni.2018.12.012 (2019).

51 Levesque, S. A. *et al.* Myeloid cell transmigration across the CNS vasculature triggers IL-1beta-driven neuroinflammation during autoimmune encephalomyelitis in mice. *J Exp Med* **213**, 929-949, doi:10.1084/jem.20151437 (2016).

52 Salmeron, K., Aihara, T., Redondo-Castro, E., Pinteaux, E. & Bix, G. IL-1alpha induces angiogenesis in brain endothelial cells in vitro: implications for brain angiogenesis after acute injury. *J Neurochem* **136**, 573-580, doi:10.1111/jnc.13422 (2016).

53 Sironi, M. *et al.* IL-1 stimulates IL-6 production in endothelial cells. *J Immunol* **142**, 549-553 (1989).

54 Thornton, P. *et al.* Platelet interleukin-1alpha drives cerebrovascular inflammation. *Blood* **115**, 3632-3639, doi:10.1182/blood-2009-11-252643 (2010).

55 Chang, C. H., Huang, Y. & Anderson, R. Activation of vascular endothelial cells by IL-1alpha released by epithelial cells infected with respiratory syncytial virus. *Cell Immunol* **221**, 37-41 (2003).

56 Di Paolo, N. C. *et al.* Virus binding to a plasma membrane receptor triggers interleukin-1 alpha-mediated proinflammatory macrophage response in vivo. *Immunity* **31**, 110-121, doi:10.1016/j.immuni.2009.04.015 (2009).

57 Lichtman, A. H., Chin, J., Schmidt, J. A. & Abbas, A. K. Role of interleukin 1 in the activation of T lymphocytes. *Proc Natl Acad Sci U S A* **85**, 9699-9703, doi:10.1073/pnas.85.24.9699 (1988).

58 Ben-Sasson, S. Z. *et al.* IL-1 enhances expansion, effector function, tissue localization, and memory response of antigen-specific CD8 T cells. *J Exp Med* **210**, 491-502, doi:10.1084/jem.20122006 (2013).

59 Jain, A., Song, R., Wakeland, E. K. & Pasare, C. T cell-intrinsic IL-1R signaling licenses effector cytokine production by memory CD4 T cells. *Nat Commun* **9**, 3185, doi:10.1038/s41467-018-05489-7 (2018).

60 Bruttger, J. *et al.* Genetic Cell Ablation Reveals Clusters of Local Self-Renewing Microglia in the Mammalian Central Nervous System. *Immunity* **43**, 92-106, doi:10.1016/j.immuni.2015.06.012 (2015).

61 Smith, D. E. *et al.* A central nervous system-restricted isoform of the interleukin-1 receptor accessory protein modulates neuronal responses to interleukin-1. *Immunity* **30**, 817-831, doi:10.1016/j.immuni.2009.03.020 (2009).

62 Strack, A., Asensio, V. C., Campbell, I. L., Schluter, D. & Deckert, M. Chemokines are differentially expressed by astrocytes, microglia and inflammatory leukocytes in Toxoplasma encephalitis and critically regulated by interferon-gamma. *Acta Neuropathol* **103**, 458-468, doi:10.1007/s00401-001-0491-7 (2002).

63 Lugrin, J. & Martinon, F. The AIM2 inflammasome: Sensor of pathogens and cellular perturbations. *Immunol Rev* **281**, 99-114, doi:10.1111/imr.12618 (2018).

64 Ruhl, S. & Broz, P. Caspase-11 activates a canonical NLRP3 inflammasome by promoting K(+) efflux. *Eur J Immunol* **45**, 2927-2936, doi:10.1002/eji.201545772 (2015).

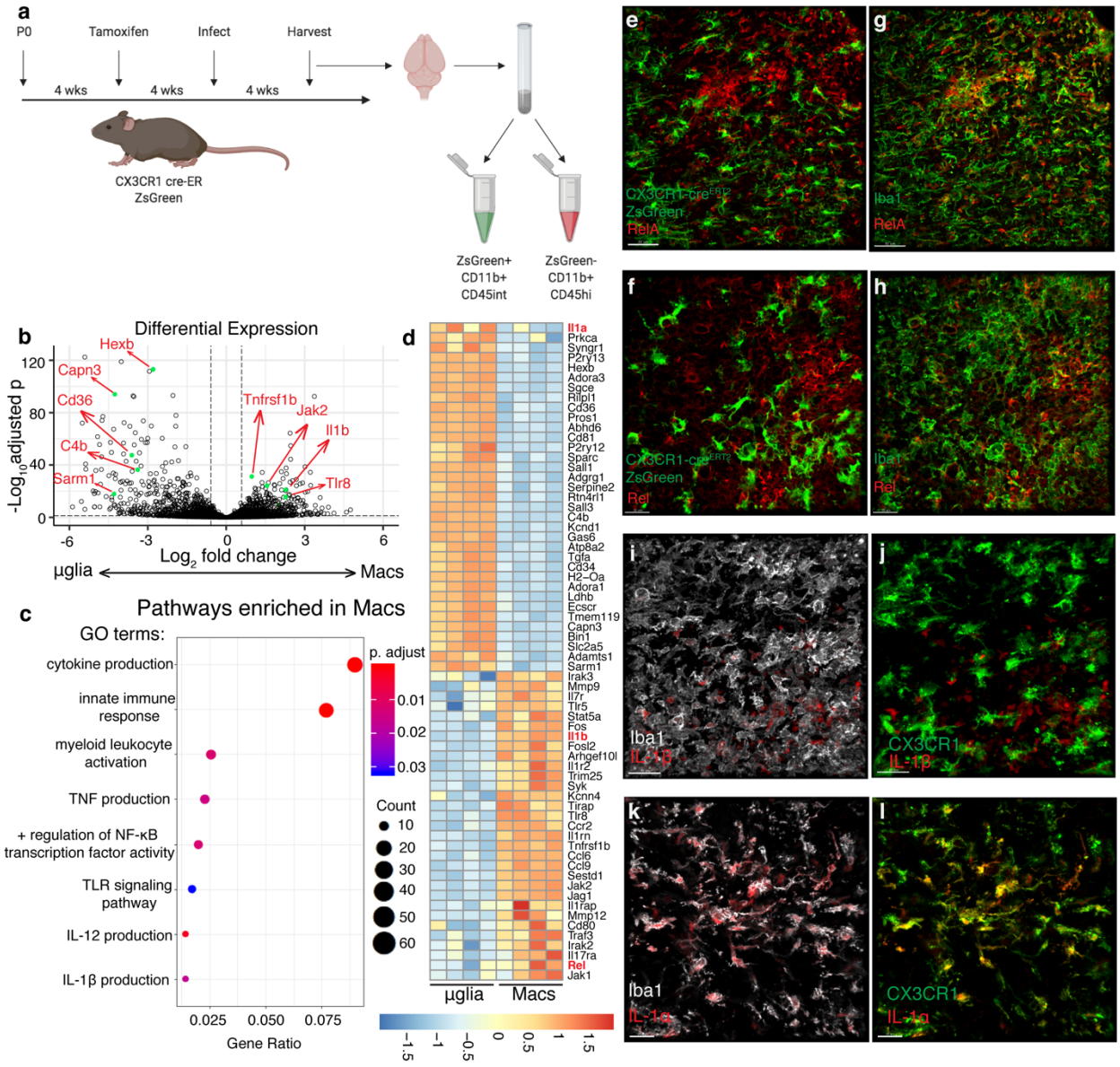

Figure 1.

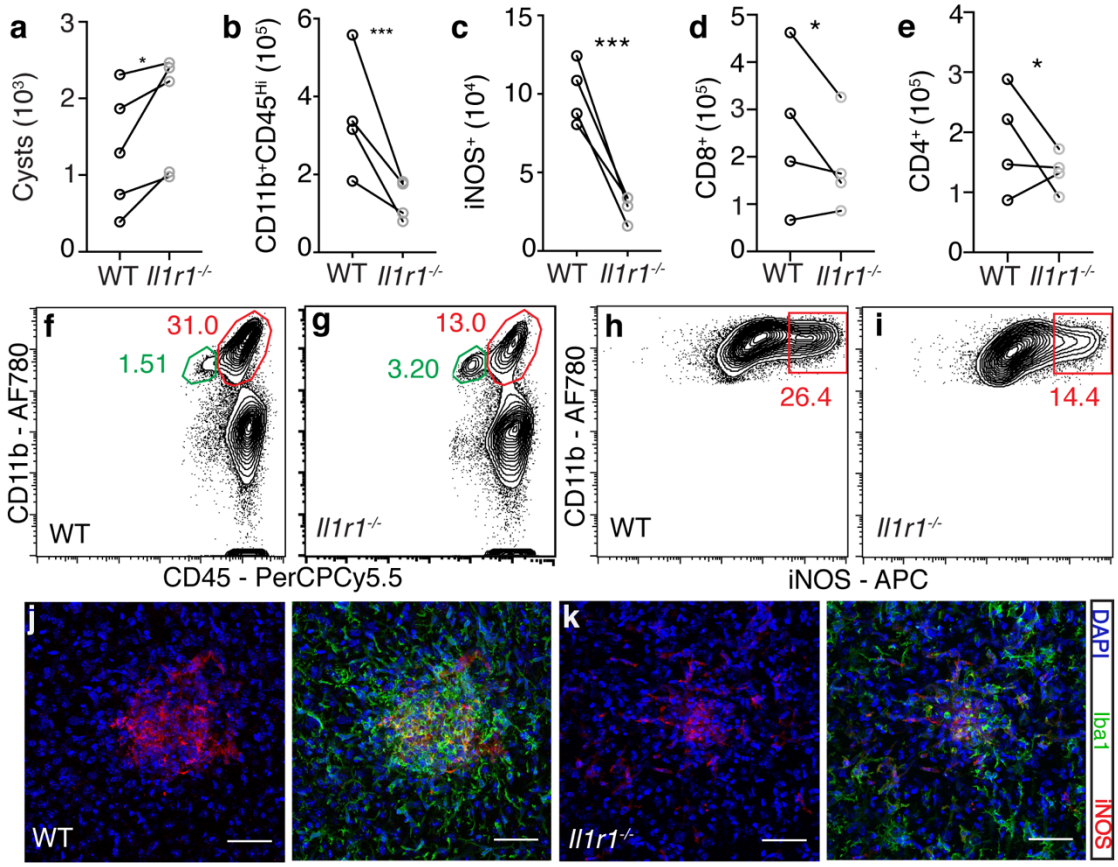

Figure 2.

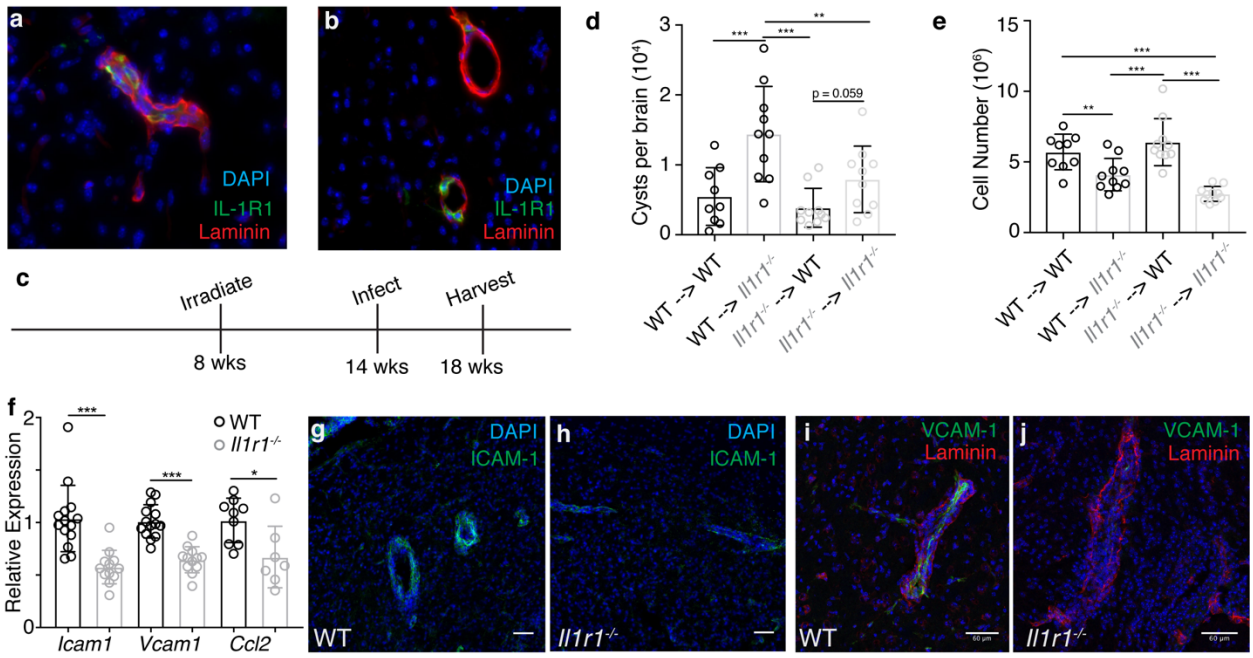

Figure 3.

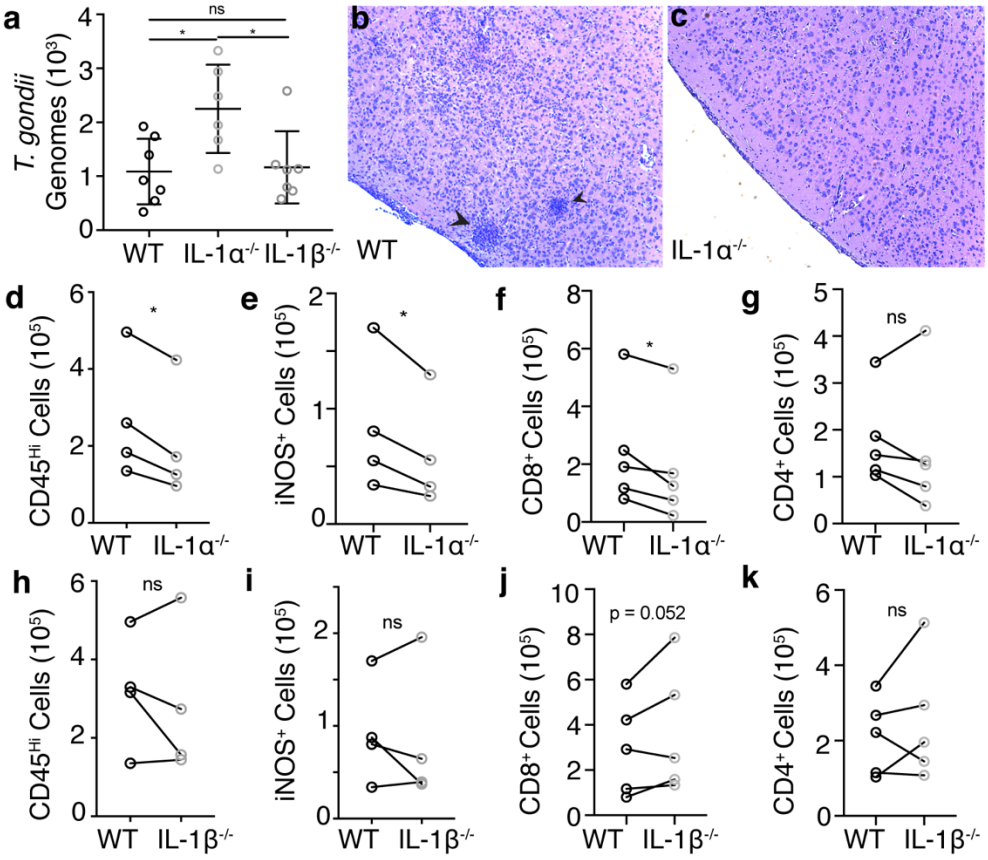

Figure 4.

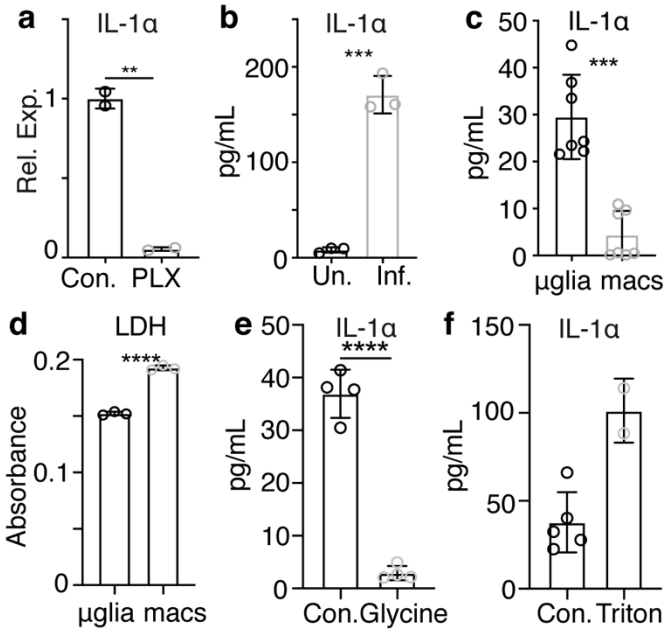

Figure 5.

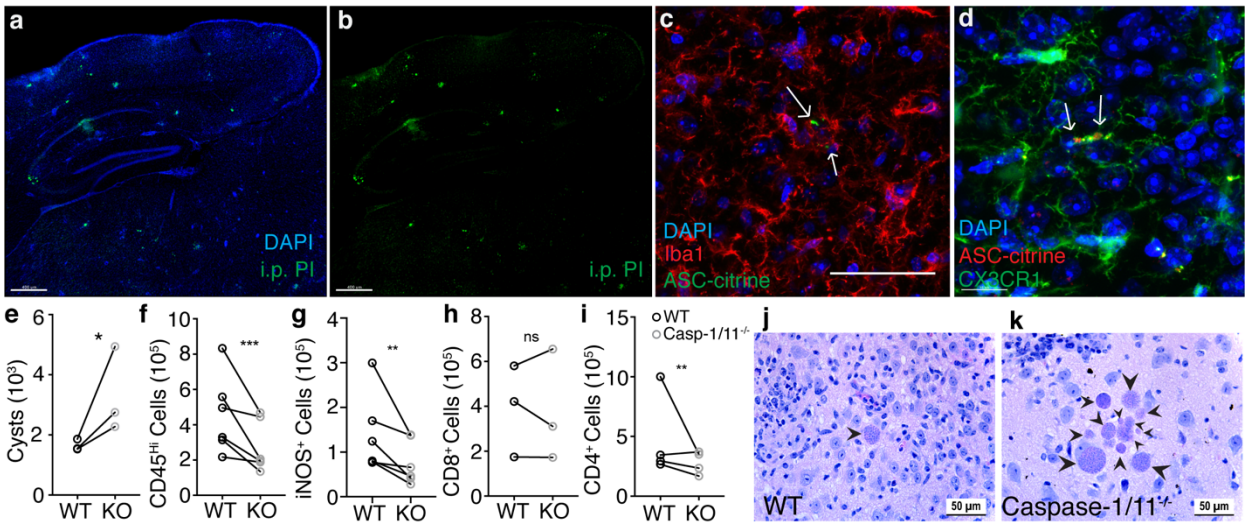

Figure 6.

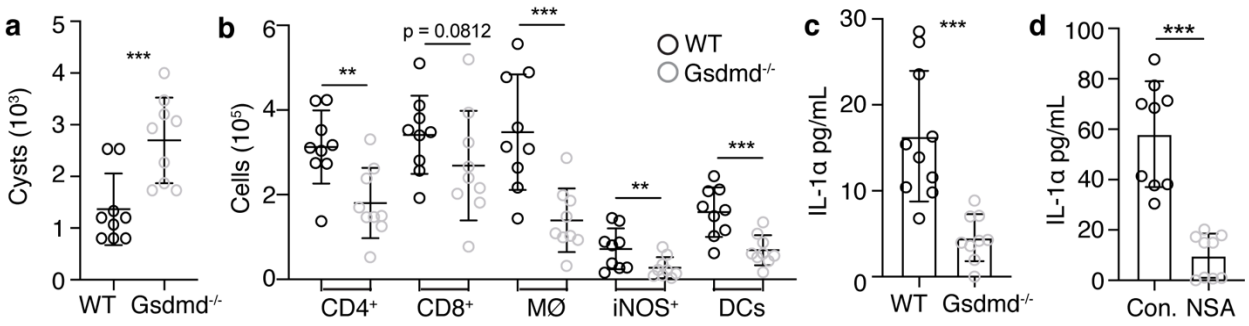

Figure 7.

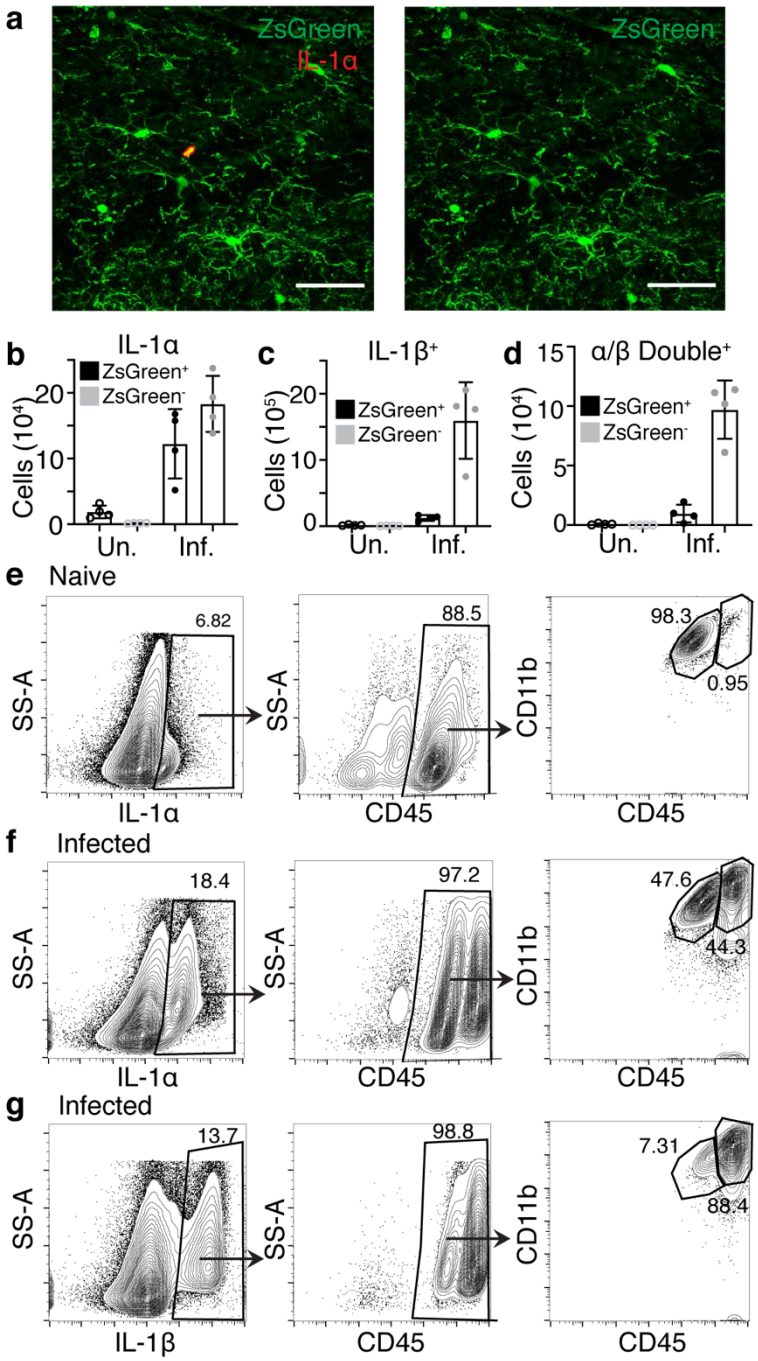

Figure S1.

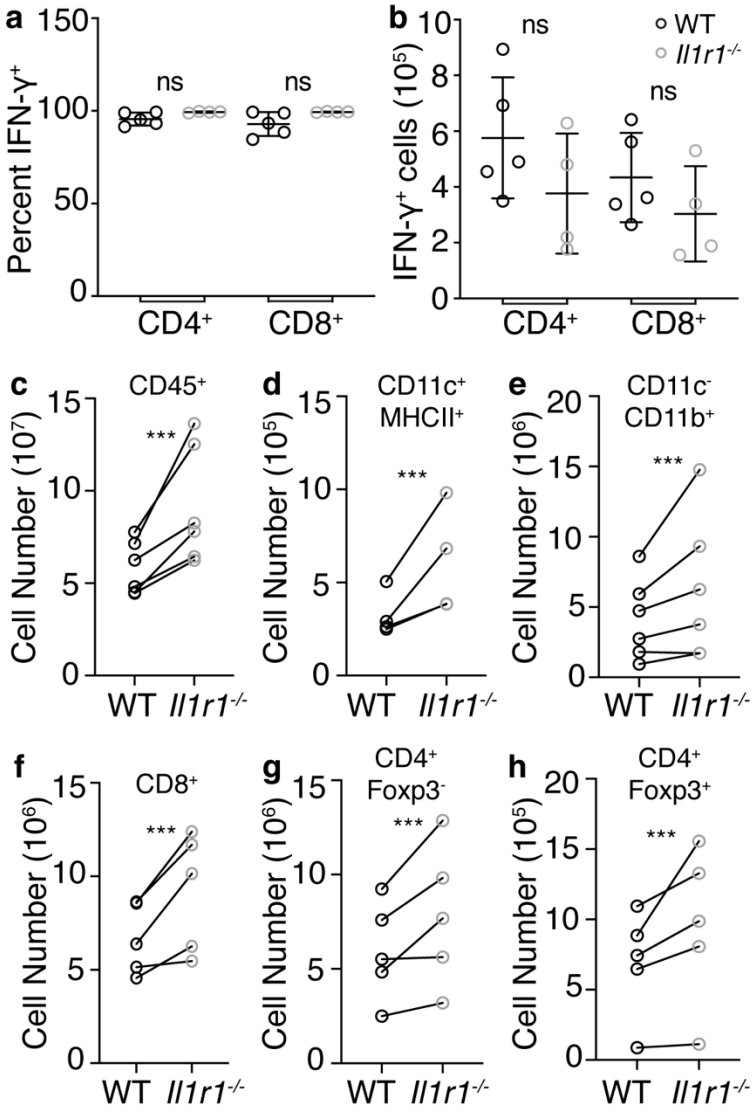

Figure S2.

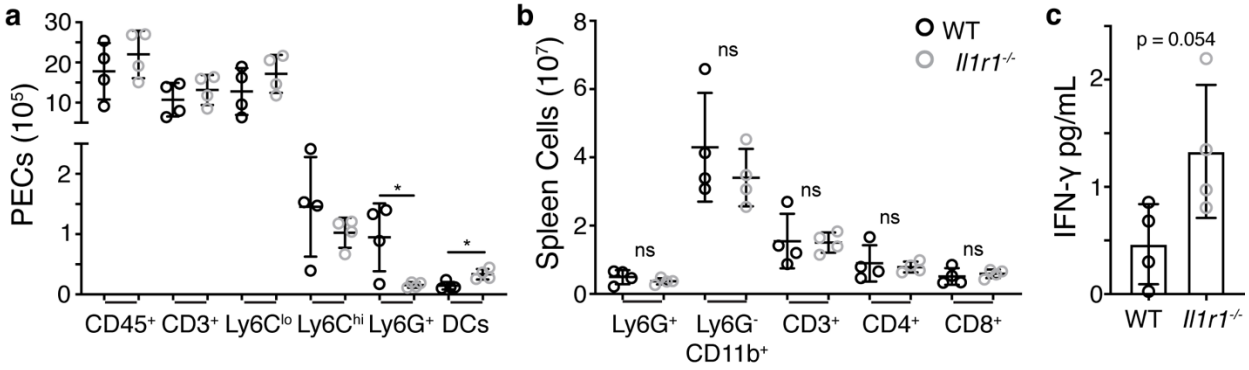

Figure S3.

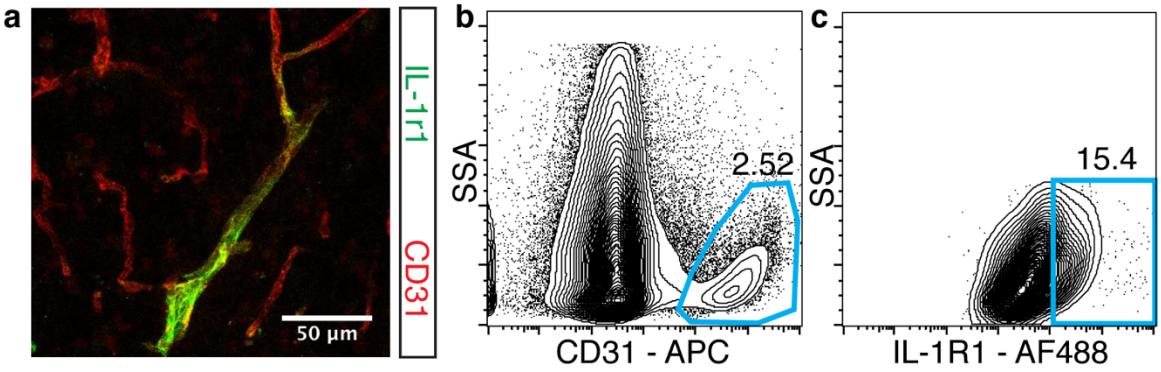

Figure S4.

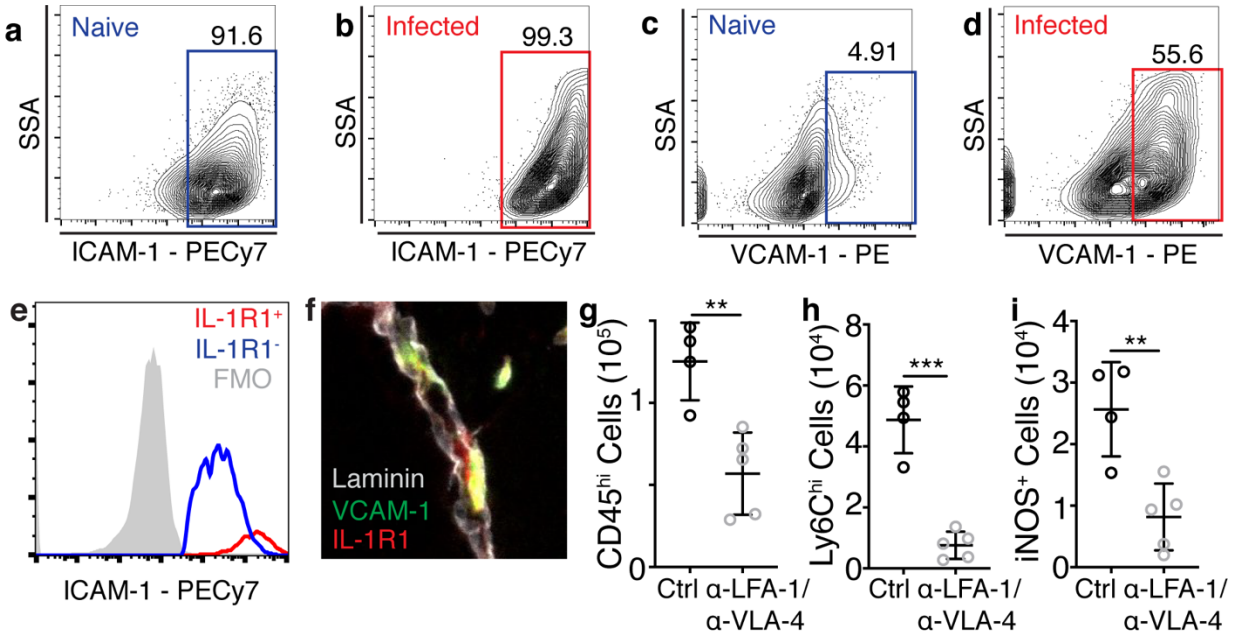

Figure S5.

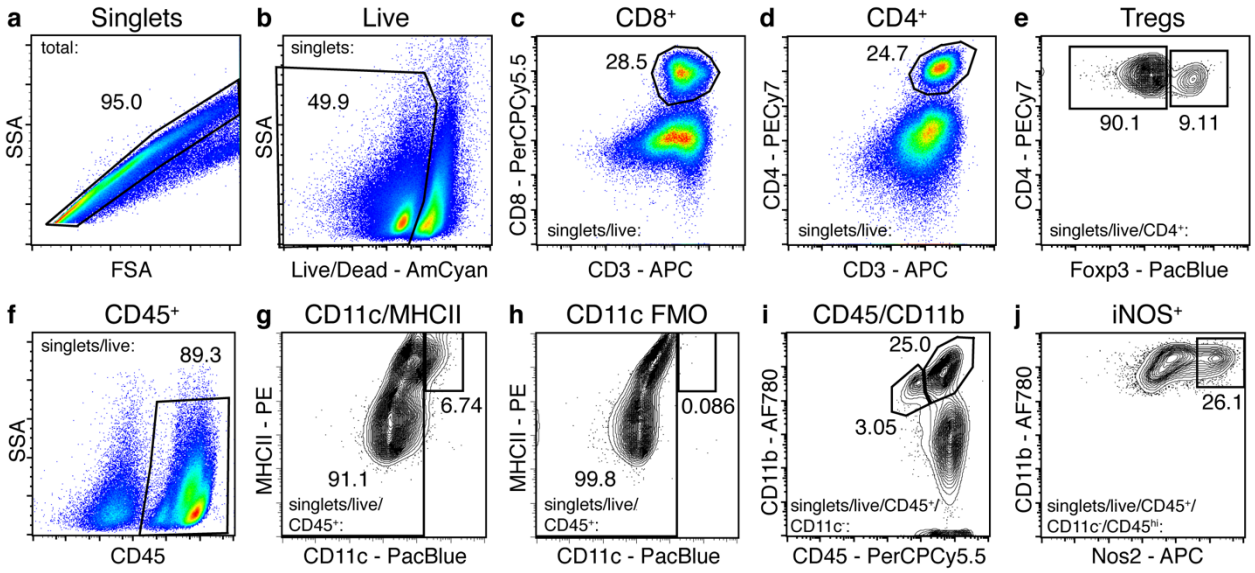

Figure S6.